공학석사 학위논문

The origin of low efficiency roll-off in OLEDs based on exciplex forming co-host system

엑시플렉스를 형성하는 공동호스트를 사용한 유기발광소자의 휘도 증가에 따른 효율 감소 현상 분석

2015년 8월

서울대학교 대학원

재료공학부 하이브리드재료 전공

심 봄 이

The origin of low efficiency roll-off in OLEDs based on exciplex forming co-host system

지도 교수 김 장 주

이 논문을 공학석사 학위논문으로 제출함

2015년 8월

서울대학교 대학원

재료공학부 하이브리드재료 전공

심 봄 이

심봄이의 공학석사 학위논문을 인준함

2015년 8월

위 원 장 조 원 호 (인)

부위원장 김 장 주 (인)

위 원 박 수 영 (인)

Abstract

The origin of low efficiency roll-off in OLEDs based on exciplex forming co-host system

Sim Bomi
Department of Materials Science and Engineering
The Graduate School
Seoul National University

Phosphorescent organic light-emitting diodes (PhOLEDs) have great potentials for applications in displays and lightings. The use of phosphorescent emitter molecules in OLEDs is essential to realize internal electron-photon conversion efficiencies of 100%. However, the efficiencies of phosphorescent OLEDs decline at high current densities – an effect known as efficiency roll-off that has been known to be mainly dominated by bimolecular interactions and charge carrier imbalance.

In this thesis, the origin of efficiency roll-off is analyzed through quantitative measuring the contribution of monomolecular and bimolecular quenching processes and charge carrier imbalance with newly modified modeling of EQE including microcavity effects and

excitons profiles. By combining electrical and optical excitation in time-resolved spectroscopic experiments, the contributions of quenching and charge carrier imbalance to efficiency roll-off are analyzed. To analyze precisely, the exciton profiles and the width of recombination zone in EML are identified by the sensing layer method based on energy transfer from the emitter to the sensitizer.

In this work, two different PhOLEDs, one with a single host, 4,4'-Bis(carbazol-9-yl)biphenyl(CBP), and the other with an exciplex-forming co-host(TCTA:B3PYMPM), are studied. Both CBP single host system and the exciplex forming co-host system have low efficiency roll-off, however the tendency of efficiency roll-off is significantly different. In exciplex forming co-host system, the high charge carrier balance and less quenching rate with wide recombination zone is the origin of low efficiency roll-off. In CBP single host system, the reduced charge balance and increased quenching rate in narrow recombination zone is mainly contribute to efficiency roll-off.

Keywords: Organic light emitting diodes, efficiency roll-off, exciplex forming co-host, exciton profile, combined electrical and optical analysis, quenching factor, charge balance factor

Student Number: 2013 - 23819

List of Figures

Chapter 1
Introduction

1.1 Motivation and outline of thesis

1.1.1 Motivation

Phosphorescent organic light-emitting diodes (PhOLEDs) have great potential for applications in displays and lightings. The use of phosphorescent emitter molecules in OLEDs is essential to realize internal electron-photon conversion efficiencies of 100% [14,15]. However, the efficiencies of phosphorescent OLEDs tends to decrease with increased current densities – an effect known as efficiency roll-off that has been known to be mainly dominated by bimolecular interactions and charge carrier imbalance [6-9].

Figure1 shows the maximum external quantum efficiency of selected OLEDs reported in the literature as a function of $J_{90\%}$. High efficiencies are mainly reported by devices based on phosphorescent emitters. However, the EQE rolls off to 90% of its maximum at currents as low as 1-30 mA/cm^2 [6]. Exciplex forming co-host system has been reported that it can be reached to its theoretical limits and the system

shows low efficiency roll-off compare to reported PhOLEDs [3-5]. The reasons of low efficiency roll-off has been investigated, however, the origin has not been reported experimentally and quantitatively at all [3,5]. Also, the commonly used CBP single host system is studied in this work because it also shows low efficiency roll-off with different roll-off shape with exciplex forming co-host system [11].

Figure1.2 shows the external quantum efficiency as functions of current density of TCTA:B3PYMPM co-host (exciplex forming co-host) and CBP single host system. The maximum EQE of exciplex forming co-host system is 29.6% and EQE decreased to 28.3% at 10000 cd/m^2 that is 95.5% of its maximum as increasing current density. The CBP single host system shows 23.5% of maximum EQE and it decreased to 17.6% at 10000 cd/m^2 that is 75% of its maximum EQE. The CBP single host system was reported as one of most reduced efficiency roll-off among reported phosphorescent green OLEDs [6,11]. Moreover, for both systems, the tendency of efficiency roll-off as functions of current density are different. The EQE of TCTA:B3PYMPM co-host system is increasing until current density is reached to 1 mA/cm^2. While the EQE of CBP single host system decreased continuously [11]. Therefore, it is able to expect that these two systems have different efficiency roll-off mechanisms.

Figure1.3 shows that the efficiency roll-off of exciplex forming co-host system cannot be explained by TTA theory which is the most

general way to explain efficiency roll-off [7]. The width of recombination zone of exciplex forming system has been considered as full length of EML (30nm in the figure). If the width of recombination zone is smaller than 3nm, the TTA theory is able to explain the efficiency roll-off. Therefore, the width of recombination zone and exciton profile of EML should be investigated to figure out mainly contributing mechanism to efficiency roll-off.

In this thesis, the origin of efficiency roll-off of both exciplex forming co-host system and CBP single host system are analyzed through quantitative measuring the contributions of monomolecular and bimolecular quenching processes and charge carrier imbalance. The main mechanisms should be investigated to understand the physics of excitons to design device structures without roll-off property in the devices and it is able to contribute to further applications.

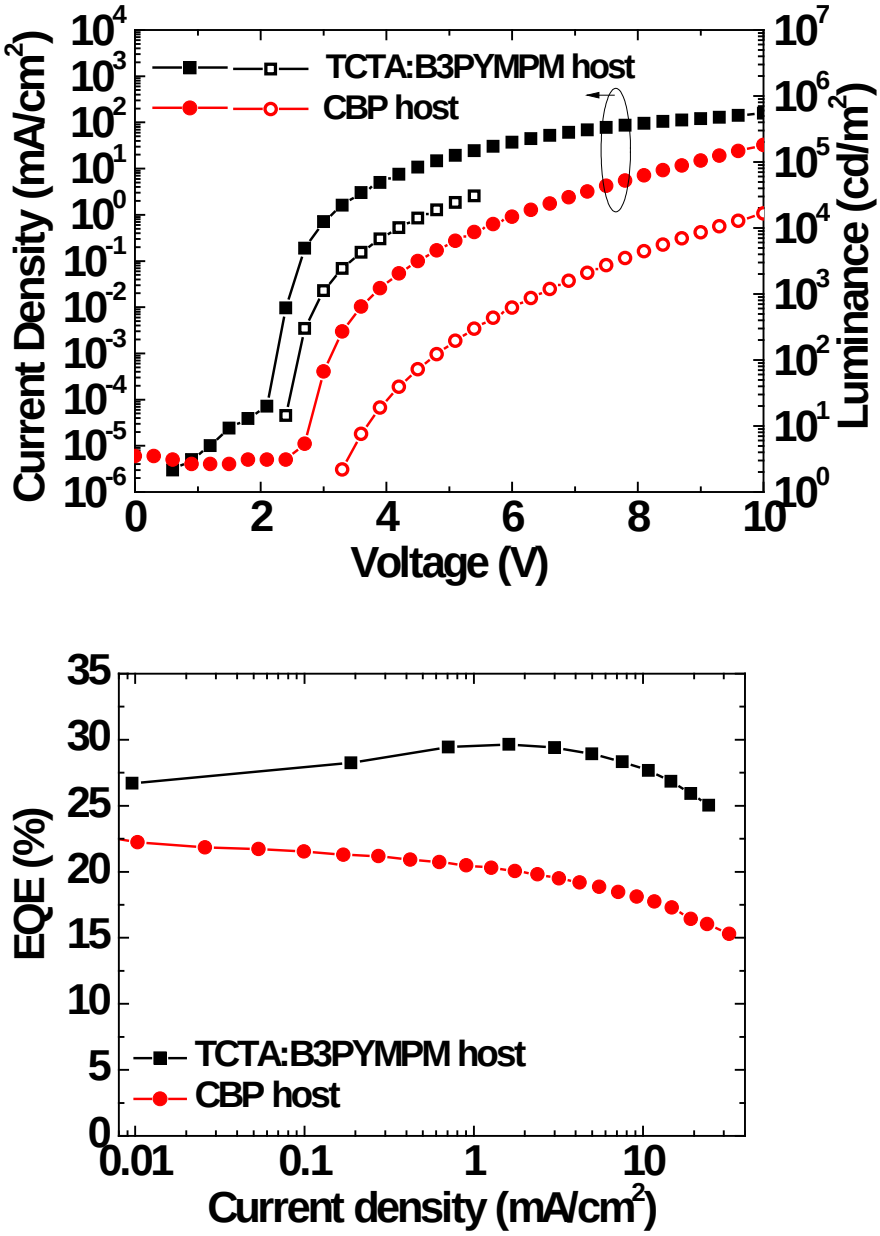

Figure 1.2. (a) The current density−voltage-luminescence (J−V−L) characteristic of exciplex forming co-host system and CBP single host system. (b) The different EQE roll-off tendency of exciplex forming system and CBP single host system

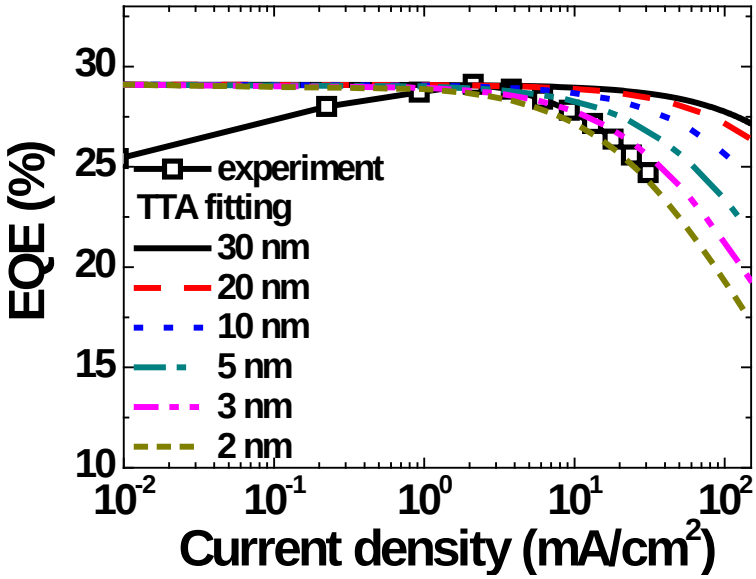

Figure 1.3. External quantum efficiency (EQE) of exciplex forming co-host system (open rectangular) and TTA fittings with various width of recombination zone (lines).

1.1.2 Outline of thesis

In chapter 1, the brief introduction of the organic light emitting diodes and operation principles of OLEDs will be described. Also the issues in PhOLEDs such as high brightness applications and the downside of phosphorescence emitter will be introduced.

In chapter 2, the processes leading to efficiency roll-off will be provided such as bimolecular quenching (TTA, TPQ) and charge carrier imbalance and exciton distribution in EML with current densities. The detail methodology to quantitative exciton profiles will be explained. The exciton distributions of exciplex forming co-host system and CBP single host system are investigated by sensing layer method. The energy transfer from emitter to sensitizer and the microcavity effects are considered. The working principle of the method will be discussed with results.

In chapter 3, the detail theory and experimental methods to quantify quenching effects and charge balance factor to explain efficiency roll-off will be introduced. The combined electrical and optical analysis was used to measure quenching factor. From the quenching factor and exciton profile, charge balance factors are calculated with a function of current density. The EQE is explained by quenching factor, charge balance factor and maximum EQE from simulation. The detail equations and experiments will be explained to discuss the results.

1.2 Organic light emitting diodes at high brightness

1.2.1 Organic light emitting diodes in brief

Organic light emitting diodes (OLEDs) convert electrical energy into light through the recombination of injected charge carriers in emitting layers of device structure. Although organic materials used to OLEDs are electrically insulator due to its large band gap about 2-3 eV and their low conductivity, OLEDs emit light quite efficiently.

The first OLED introduced by Tang et al. was composed of bi-layered organic structures with electron transporting layer (ETL) and hole transporting layer (HTL) [1]. The efficiency of the device was very low(<1%) because it harvested only the fluorescence from a singlet exciton due to the forbidden relaxation of triplets in the device.

To harvest triplet exciton, Baldo et al. introduced PtOEP (2, 3, 7, 8, 12, 13, 17, 18-octaaethylporphine platinum) dye [16]. The heavy metal complex emitted phosphorescent light due to strong spin-orbit coupling. This was the first phosphorescent OLED (PhOLED) and is regarded as the second generation of OLEDs. After their pioneering work, the way to achievement of 100% internal quantum efficiency (IQE) of the OLEDs is opened and the efficiency of PhOLEDs has been significantly improved (by 30%) [3,17,18]. However, PhOLED still have many issues to overcome because the efficiency is declined at

high luminescence level.

1.2.2 Operating principles of the OLEDs

A bottom emitting OLED consists of a transparent anode (ITO) on top of a glass substrate, followed by hole transport layer (HTL), emitting layer (EML), electron transporting layer (ETL), and a reflective metallic cathode, finally capped with encapsulation for a higher operating stability in an inert environment. Currently, highly efficient OLEDs have become complex multilayer structures to have various functions such as charge transporting, exciton formation, energy transfer, recombination, and so on. The physical processes in OLED are injection of holes from a high work function anode into the highest occupied molecular orbital (HOMO) of a HTL and electrons from cathode into the lowest unoccupied molecular orbital (LUMO) of the ETL through an electron injection layer. After then, the oppositely charged carriers are transported through a HTL and an ETL towards an EML each other under the applied electric field. The injected holes and electrons into an EML make recombination in the EML and forms excitons. The formed exciton transfer their energy to emitting dyes (which is optional) and they decay radiative to emit.

The external quantum efficiency (EQE) of OLED is defined as the ratio of the number of emitted photons to the amount of charge injected

into device, and can be expressed by the following equation [4, 19].

$$\eta_{EQE} = \gamma \times \eta_{s/t} \times q_{eff}(\phi_{PL}, \Theta, \Gamma) \times \eta_{out}(\Theta, \Gamma) \quad (1)$$

Here, γ is the charge balance factor, which explain exciton formation efficiency from injected carriers. $\eta_{s/t}$ is the ratio of single to triplet excitons ($\eta_{s/t}$ = 1/4 for fluorescent, $\eta_{s/t}$ = 3/4 for phosphorescent emitters), q_{eff} is the effective radiative quantum yield which is conversion efficiency of excitons to photons. η_{out} is the out-coupling efficiency of the emitted light that is ratio of out-coupled photons to generated photons. Using eq. (1), a maximum EQE has been predicted at 46% for green phosphorescent OLEDs (PhOLEDs) with the horizontally-oriented emitter [4].

1.2.3 Exciplex-forming co-hosts for OLEDs

In organic semiconductors, the electronic excited states are different from those in inorganic semiconductors. In contrast to the Mott-Wannier excitons in a tightly bonded inorganic semiconductor, there are high enough binding energy of excitons in an organic semiconductors [20]. A charge-transfer exciton (CT exciton) have two kinds of bimolecular excitonic excited state, one is an excited dimer (excimer) and another is an excited complex (exciplex) [20]. When donor and

acceptor molecules approach each other, they are dissociative at ground state because of steric hindrance. However, when an excited molecule (D* or A*) bind to another ground state molecule (D or A), the two molecules approach due to the charge transfer interactions. The exciplex-forming co-hosts system has been proposed for break through system that overcomes all the barriers to realizing the ultimate efficiency in OLEDs in terms of the high EQE, low driving voltage and low efficiency roll-off [3-5]. Figure 1.4 shows the schematic device structure with energy diagram using an exciplex-forming co-host system composed of a hole transporting material (TCTA) and an electron transporting materials (B3PYMPM), which are used for a HTL and an ETL, respectively [4,5]. In this exciplex forming system, electrons and holes reach to EML without energy barriers. The oppositely charged carriers are recombined in the EML forming an exciplex. The formed exciplex on the co-hosts, transfer their energy into phosphorescent dyes. The triplet energies of the HTL, ETL, and the exciplex are higher than that of dyes, the excitons are well confined inside EML.

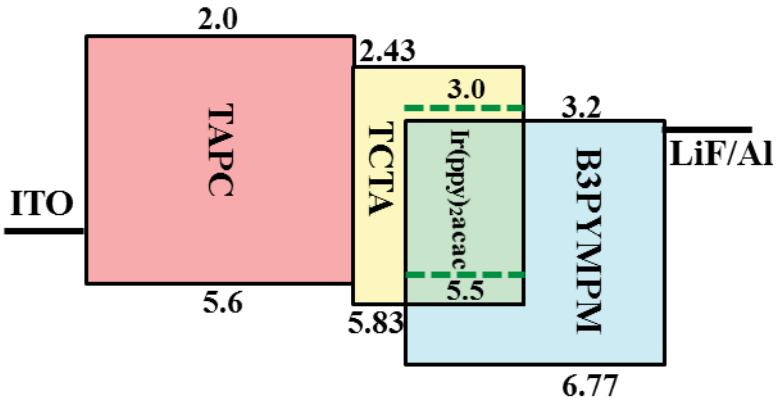

Figure 1.4. The schematic device structure with energy diagram using an exciplex forming co-host (TCTA:B3PYMPM) composed of a hole transporting materials (TCTA) and an electron transporting material (B3PYMPM)

1.2.4 Issues in PhOLEDs

Phosphorescent organic light-emitting diodes (PhOLEDs) have great potential for applications in displays and lightings. The use of phosphorescent emitter molecules in OLEDs is essential to realize internal electron-photon conversion efficiencies of 100% [14,15]. This is essential to application of large area displays of lighting which need higher levels of luminescence. To maintain high luminescence, high voltages should be applied consistently. However, the efficiencies of phosphorescent OLEDs tends to decrease with increased current densities – an effect known as efficiency roll-off that mainly dominated by bimolecular interactions and charge carrier imbalance. Therefore, the importance challenge for high-brightness applications is to reduce the efficiency roll-off in PhOLEDs.

To systematically reduce the efficiency roll-off mechanisms, detailed fundamental studies have been performed, but the mechanisms are not fully understood in many cases.

In this regard, detailed description of the different mechanisms leading to efficiency roll-off will be introduced in next section.

1.2.5 Processes leading to EQE roll-off in OLEDs

In terms of efficiency, PhOLEDs can compete with highly efficient conventional light sources but their quentum efficiency typically decreases at high current densities level, an effect know as efficiency roll-off [7]. For the mechanisms to leading to efficiency roll-off, bimolecular interactions such as triplet-triplet annihilation (TTA), triplet-free electron and triplet-free hole quenching (TPQ) have been studied from may groups [6,7,8]. Also, charge carrier imbalance is one of important mechanisms to reduce efficiency at high current densities level. In this reagard, the processes leading to EQE roll-off in OLEDs will be introduced briefly.

Bimolecular interactions

The electron to photon conversion efficiency of PhOLED at high brightness level is may decreased by bimolecular quenching between excitons. TTA(triplet-triplet annihilation) is mostly relevant to the efficiency roll-off in phOLEDs. In 2000s, Baldo and co-workers investigated the efficiency roll-off mechanisms in particular TTA such as host-guest triplets interactions [7]. In Eq. (2) the annihilation of two triplet states leads to an intermediate state X, which is able to be transferred into one singlet or tree triplets.

$$\begin{aligned} T_1 + T_1 \xrightarrow{k_{TT}} X \xrightarrow{75\%} T_n + S_0 \rightarrow T_1 + S_0 \\ \xrightarrow{25\%} S_n + S_0 \rightarrow S_1 + S_0 \end{aligned} \quad (2)$$

Where k_{TT} is the rate constant of TTA process. In PhOLEDs system, the TTA process is mainly depends on the triplet density and the excited state lifetime. Owing to the relatively longer lifetime of phosphorescent than fluorescent materials, the possibility of interations is higher which leads significantly decrease of the efficiency in PhOLEDs.

One of the most dominent processes is the interaction of triplet excitons with free charges refereed to as triplet-polaron quenching (TPQ) [8]. Such process can be expressed by folowing expression,

$$\begin{aligned} T_1 + h^+ \xrightarrow{k_{TP},h} S_0 + h^{+*} \\ T_1 + e^- \xrightarrow{k_{TP},e} S_0 + e^{-*} \end{aligned} \quad (3)$$

Where electrons (e^-) and holes (h^+) and their respective annilation rates $k_{TP,h}$ and $k_{TP,e}$. The star denotes higher excited states. When triplet excitons interact with free-carriers, the complexes become higher excited state and the triplet excitons relax into ground state (S_0)

Charge carrier imbalance

Besides quenching of excitons, the efficiency of the exciton generation

processes also depend on the current densities, thus considering as further potential source of efficiency roll-off. At low current densities, charge imbalances can be explained by the difference energy barreirs of electrons and holes inside the device structure [21,22,23]. At higher current densities, the charge carrier imbalance is reduced as injection barriers are easier to overcome [24,25]. However, if the injection barreirs are field depentdent, the charge balance is decreased as increasing current density which leads efficiency roll-off [9,26].

In a device structure, the charge balance factor, b, is represented as below [21,22]:

$$b = \frac{J_{h,anode} - J_{h,cathode}}{J} = \frac{J_{e,cathode} - J_{e,anode}}{J} \quad (4)$$

The charge balance factor is considered as exciton formation efficiency that is the probability of hole or electrion injected into the emissive layer recombines before exiting. The effect of charge carrier imbalance on efficiency roll-off has little been studied [9]. Moreover, the exciplex system has not been studied at all in that quantitivly analysis of the origin of efficiency roll-off. In this regards, the effect of charge imbalance and quenching on efficiency roll-off for exciplex forming system will discussed in following chapters.

Chapter 2

Investigation the role of exciton profiles in OLEDs

2.1 Introduction

One of the important issues of OLEDs is exciton distributions in emissive layer of OLEDs [27]. The locations of excitons affect to effective quantum efficiencies and out-coupling efficiencies that are closely related to EQE of OLEDs [4]. Moreover, the reduction in confinement of charge carriers in EML at high current density level causes the efficiency roll-offs because the amount of excitons that are able to radiative decay are reduced in the EML [9]. The hole or electron blocking layers (HBL, EBL) can be used to prevent such loss mechanisms. Also, exciton confinement is important to reach high efficiency. Therefore, exciton profiles in EML and width of exciton formation zone are critical to understand the physics of mechanisms of performance of OLEDs.

Recently, the correlations of exciton profiles and efficiency roll-off have been reported. R. J. Homles et al. studied that the impact of the exciton recombination zone width on the quenching mechanisms in various OLED architectures [27]. They found that in a graded-emissive layer based OLEDs which is known as G-EML, the efficiency roll-off

is mainly due to both triplet-triplet annihilation (TTA) and triplet-polaron quenching (TPQ), while in conventional double layer based OLEDs the roll-off is mainly dominated by TTA, only. The result is explained by the larger exciton recombination zone in G-EML devices, which have less exciton density-driven quenching at high current densities level. Also, they consist that the larger exciton recombination zone plays in mitigation the roll-off.

It has been reported that exciplex forming co-host system has broad exciton recombination zone which affects reduced efficiency roll-off [3-5]. The emission spectrum of exciplex system is not shifted at high exciton densities level. As free holes and electrons hardly exist in EML and the wide width of recombination zone, triplet-polaron interaction are well prohibited in exciplex forming co-host system.

However, the exciton profiles of exciplex forming co-host system had not been reported experimentally. Moreover, to understand exciton behavior of exciplex system, the profile should be investigated.

In this chapter, firstly, investigating emission profiles by sensing layer method will be introduced. Secondly, a microcavity effect of photon will be discussed to identify exact exciton distributions. Then, exciton profiles will determined with consideration of energy transfer from green emitting dopants of the exciplex systems ($Ir(ppy)_2acac$) to sensitizer ($Ir(mphmq)_2tmd$). The calculated Forster radius will be resolution of the method. Also, the exciton profiles of CBP single host

system will be investigated with same methodology.

2.2 Sensing layer methodology

To investigate the width of exciton recombination zone in EML, the emission profile should be figured out. The emission profile can be probed directly through the addition of a sensing layer which capable of energy transfer of exciton formed on the emitter at different locations within the EML [8]. Figure 2.1 shows the schematic of sensing layer method. By comparing PL intensity of the samples at peak wavelength of the sensitizer (604nm), the maps of excitons will be shown. The PL spectra of a sample without sensing layer shows only green color emission (peak at 524nm) while the samples with a sensing layer show red color emission (peak at 604nm) because the green emitted excitons transferred to the red emitted excitons through the Forster energy transfer mechanisms [28,29,30]. Once the exciton is transferred from the emitter to the sensitizer, it will be detected by monitoring the emissions from the sensitizers. The Forster energy transfer radius of excitons from dopants ($Ir(ppy)_2acac$) molecules to sensitizer ($Ir(mphmq)_2tmd$) is 2.5nm [30]. Therefore, 5nm is the resolution of each sensing layers. The device structures and sensing layer method are in figure 2.2. For the method, 8 different devices was fabricated that

including reference device (without a sensing layer), sensing strip located at 0nm, 5nm, 10nm, 15nm, 20nm, 25nm, 30nm along with the resolution was calculated as 5nm. Therefore, each devices has a sensing layer at different positon except reference device. To quantitative measure of the emission profiles, mainly two conditions need to be fulfilled. Those are that; (1) The additional layer should not affect the transport properties of the reference device and (2) the energy transfer should be a locally confined process [8]. To fulfill (1), the sensing layer should be kept to thin with effective thickness of 0.5nm which does not form a closed layer. It can be detected from J-V curves which are almost identical with that of reference device. It means that the additional layer not substantially alter the natural distributions of charge carriers or excitons within the device. For condition (2), the resolution should be considered. The Forster energy transfer from the emitting dopants ($Ir(ppy)_2acac$) to the sensitizer ($Ir(mphmq)_2tmd$), and thus the spatial resolution of distance of the exciton transfer, may be affected by selecting sensitizing material with an appropriate overlap of absorption with the emitters.

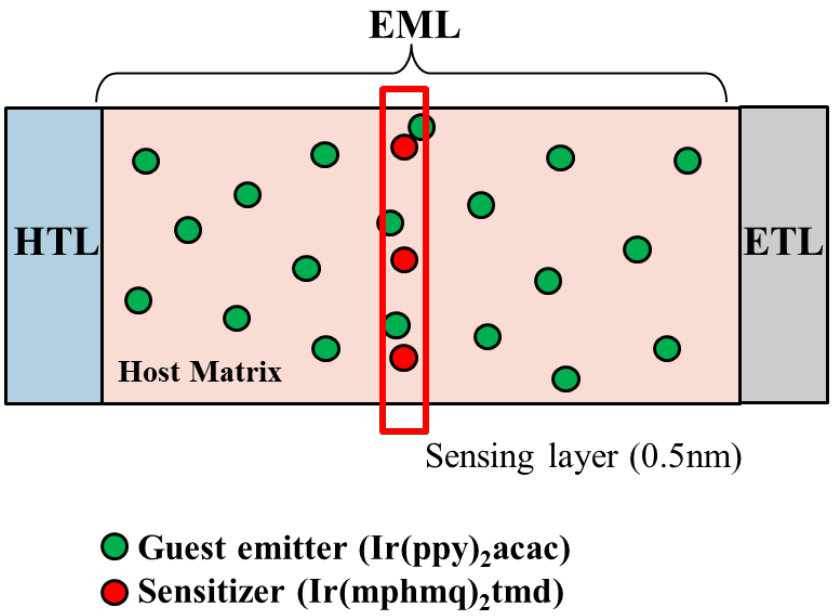

Figure 2.1. The scheme explains sensing layer method. The additional layer which have sensitizer prove the location of dopants excitons by Forster energy transfer.

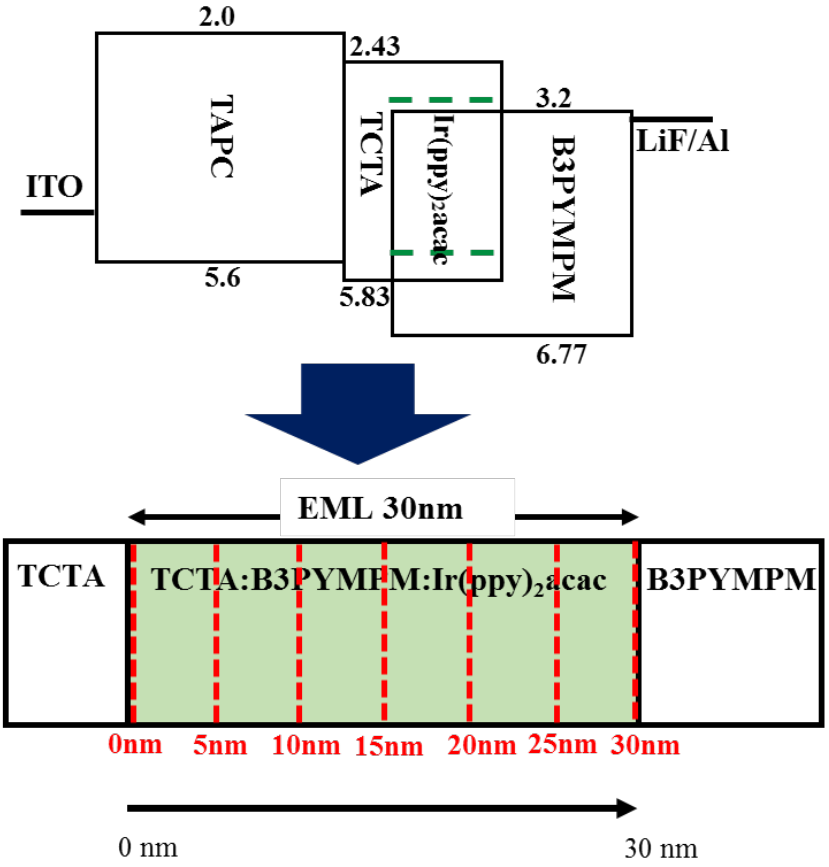

Figure 2.2. The device structures and sensing layer method of exciplex forming co-host system. ITO (70nm)/ TAPC (75nm)/ TCTA (10nm)/ TCTA:B3PYMPM:8wt% $Irppy_2acac$ (30nm)/ B3PYMPM (45nm)/ LiF (1nm)/ Al (100nm). Including a reference sample, 8 different samples are fabricated that include a sensing layer at different positions in EML. The resolution is 5nm owing to the calculated Forster radius of the excitons is 2.5nm.

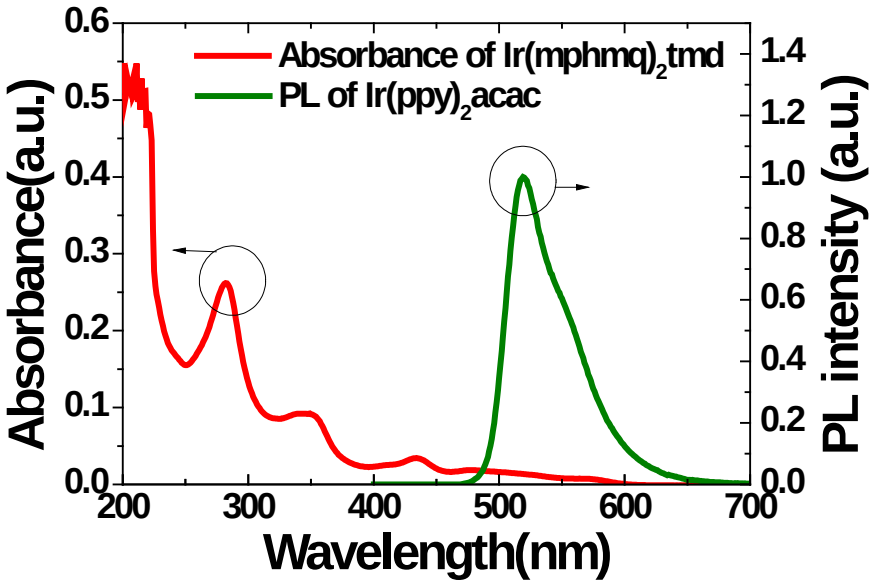

Figure 2.3. The absorbance of the sensitizer ($Ir(mphmq)_2tmd$) and PL spectrum of the emitting dopants ($Ir(ppy)_2acac$). The Forster radius is 2.5nm as overlap of the spectra is small enough to ensure spatial resolution.

Figure 2.3 shows the spectra overlap of absorbance of $Ir(mphmq)_2tmd$ (sensitizer) and PL intensity of $Ir(ppy)_2acac$ (emitter). It is analyzed to calculate the Forster energy transfer radius from the emitter to the sensitizer [30].

The Forster energy transfer is a resonant dipole coupling between a donor (emitter) and an acceptor (sensitizer) molecule with long range energy transfer (<10nm). It must be allowed donor and acceptor transitions (S-S. S-T, T-T) [30].

The PL spectra of $Ir(ppy)_2acac$ molecules shows small spectrum overlap with the absorption spectra of $Ir(mphmq)_2tmd$. The Forster transfer radius (R_0) is the characteristic distance at which the efficiency of transfer is 50% [30].

$$R_0^6 = \frac{9\eta_{PL}\kappa^2}{128\pi^5 n^4}\int \lambda^4 F_D[\lambda]\sigma_A[\lambda]d\lambda \qquad (2)$$

Where η_{PL} is the photoluminescence efficiency of the donor, κ is the dipole orientation factor, n is the index of refraction of the medium between the donor and acceptor, λ is the wavelength, F_D is the area-normalized donor emission spectrum, and σ_A is the absorption cross-section of the acceptor. The Forster energy transfer radius between the emitter and the sensitizer is considered as the spatial resolution of exciton transfer between the emitter and sensitizer, and thus it can be

tuned by selecting appropriate sensitizing material with an overlap of the absorption with the emitter emission. The energy transfer then occur over a small distance (2.5nm) and fulfill a high sensitivity to the presence of guest excitons with thin sensing strip (0.5nm). Such a thin layer is unlikely to affect charge transport and leads to only a slight reduction in spatial resolution.

In this work, the analysis of the emission profiles in EML of exciplex forming co-host system and CBP single host system is conducted by including a high sensitivity and high degree of spatial resolution of a sensing layer into a device to detect the excitons forms on the $Ir(ppy)_2acac$ (emitter) molecules via Forster energy transfer. Here, $Ir(mphmq)_2tmd$ is selected based on the small overlap of its absorption cross section with PL of $Ir(ppy)_2acac$. The sensitizer has lower triplet energy level compare to that of $Ir(ppy)_2acac$. This ensure that excitons transferred from $Ir(ppy)_2acac$ to $Ir(mphmq)_2tmd$ predominantly. The relative emission intensity from the red-emitting sensing layer can provide information about the spatial distribution of excitons in the EML. Using an equation (2) and the optical properties of the molecules, R_0 was calculated as 2.5nm and the resolution of the sensitizer is 5nm because a sensing layer may detect excitons from left and right side. Here, the sensitizer is co-deposited at 5wt% at different positions separated by 5nm in the EMLs with width of 0.5nm.

Owing to the narrowness of the sensing layers, their presence should

not significantly affect the charge transport or the recombination properties in the EML. This is confirmed by the almost identical J-V characteristics between devices with and without sensing layers. Figure 2.4 shows current-density-voltage characteristics (J-V) for the exciplex forming co-host system with a sensing layer located at different position within the EML. The reference device which does not containing a sensing layer is shown in black rectangular symbols. To ensure that the additional sensing layer do not alter the natural distribution of excitons, the current density of each sensitized device at various current density is plotted as function of sensitizer position. For all devices, current density is almost identical with reference device.

To determine the exciton distribution in EML, one of the important factors should be included that is microcavity effect. The excitons at different positions in the device structure affect to far-field extraction efficiency of excitons. In this regards, the microcavity effects will be discussed in the following section.

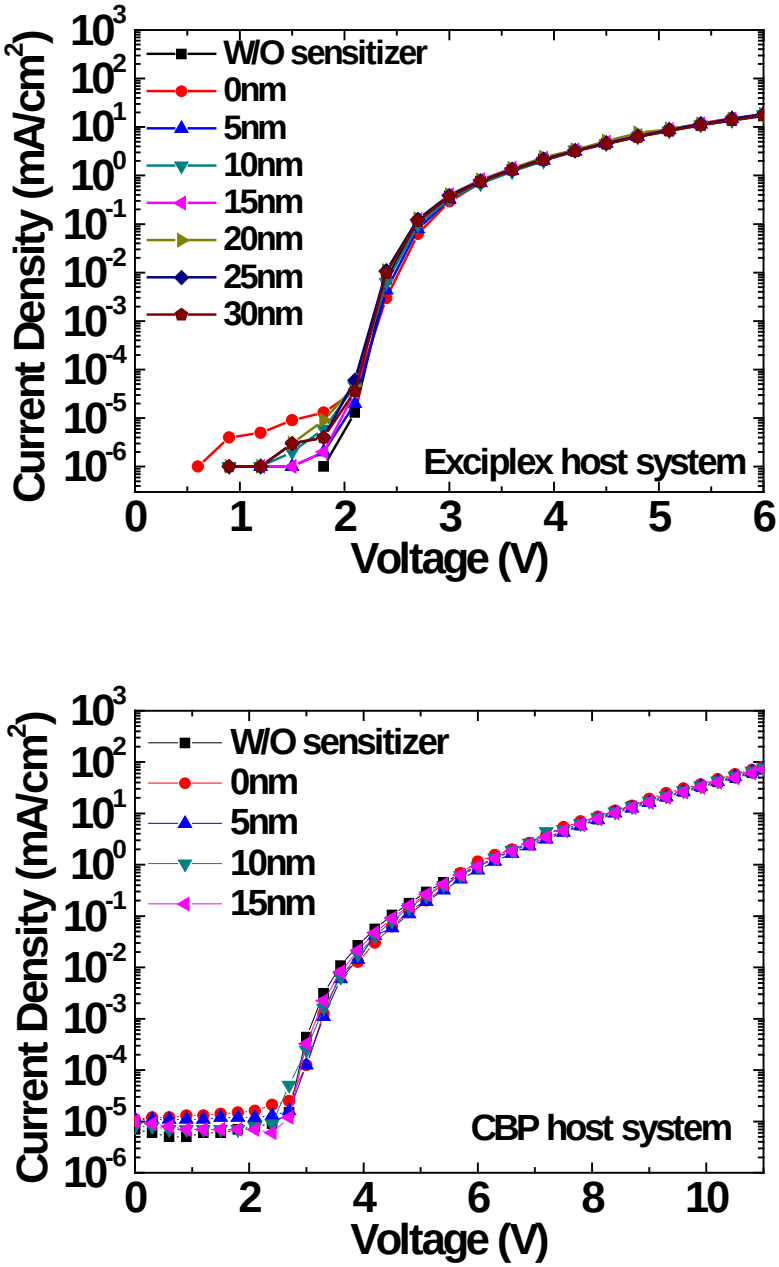

Figure 2.4. The J-V characteristics of devices; (a) exciplex forming co-host based device (b) CBP single host based device. The J-V properties are almost same as reference device (W/O sensitizer).

2.3 Exciton profiles in a microcavity structure

Determining the precise shapes of the exciton distribution in the EML is important to understanding of the physics of the exciton mechanisms. To investigate accurate shape of the emission profile, the microcavity light out-coupling model has been used [31,32,33].

Figure 2.5 (a) shows the microcavity structures of the exciplex forming system. The emission profile through the sensing layer method give us detected exciton intensities that transferred from emitter to sensitizer. However, even though same amount of excitons are existed at various positions at EML, the out-coupled EL intensities can be detected differently [31]. This is because of the microcavity effect of exciton in the device structure. The optical analysis was conducted to map the exact exciton profile from the emission profile [31-33].

Figure 2.5 (b) shows the mechanisms that a dipole (P) inside a cavity structure emit out-side of the cavity structure (P_{out}) and the intensity ($I(\Theta)$) is detected from the emitted dipole with angle Θ from normal. Figure 2.5 (c) illustrate the detected intensity from various angle of emitted. The sum of out-coupled dipole energy (P_{out}) can be consisted as be inside a spherical condition [31]. To calculate sum of the detected light intensity with angle Θ, it is integrated by the mensuration by division. To correlate with experimental, the only light from normal

angle was considered (Θ=0).

The number of excitons in a cavity structure is calculated by below expression.

$$\#\text{of exciton} \times P_0 \times \frac{2\pi r^2 I_0}{P_0} \propto \text{EL intensity} \tag{3}$$

$$F_{out} = \frac{P_{out}}{P_0} = \frac{2\pi r \int_0^{\pi/2} \sin\theta \cdot I(\theta) d\theta}{P_0} \tag{4}$$

$$F = \frac{P}{P_0} \tag{5}$$

$$\eta_{out} = \frac{P_{out}}{P} \tag{6}$$

Where, P_0 is a dipole energy inside a cavity structure, P_{out} is a sum of out-coupled dipole energy, I_0 is detected intensity from normal (Θ=0), F is purcell factor, F_{out} is purcell factor for out-coupled power [31].

To determine the number of excitons at various locations with consideration of a microcavity effect, the measured intensity is needed to be divided as express (3).

(a) (b)

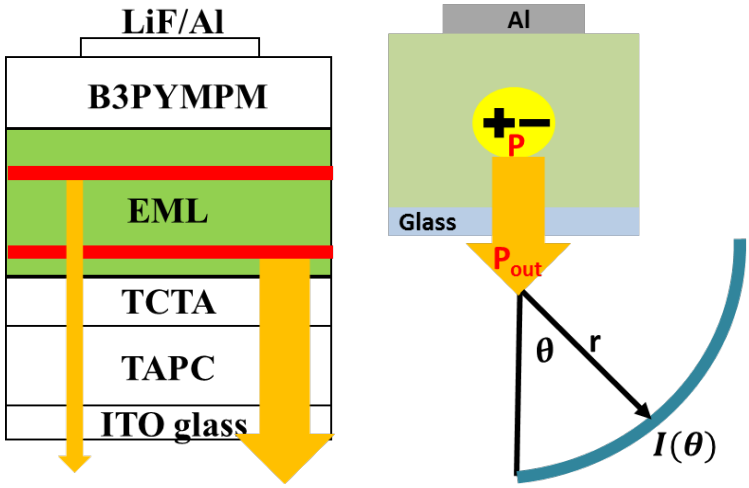

(c)

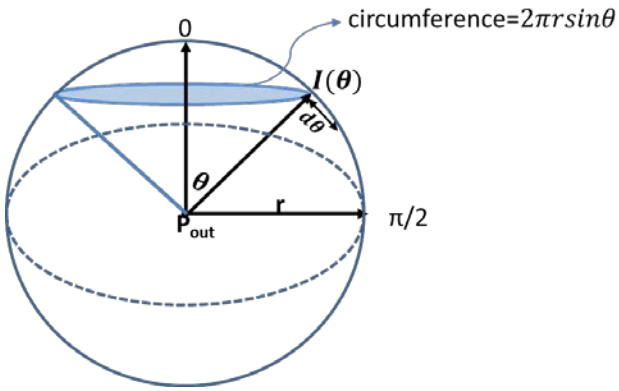

Figure 2.5. The microcavity effect of the device. (a) scheme for explain the microcavity structure of exciplex forming co-host based device (b) scheme for illustrating relation of detected intensity (I(Θ)) and dipole inside EML. (c) Scheme for illustrating intensity with various angle of detect.

2.4 Result and Discussion

Figure 2.6 shows the measured EL spectra of sensitized devices and reference device as a function of position of a sensing layer for the two system. The emitter ($Ir(ppy)_2acac$) has a peak near 524nm and the peak of the sensitizer is located at 604nm. To investigate the exciton profile, only red exciton intensity should be counted owing to the only red emission represents proved excitons at the locations. Figure 2.8 shows the discrepancy of exciton density with various locations when the red spectrum is used to determine exciton profile or when the red and green emission both are used. When we use both of red and green emission at 604nm, the exciton densities are overestimated. Therefore, the spectrum should be divided into green and red portion. Figure 2.7 shows that calculated EL spectra of green and red emission. First of all, the green spectra is calculated from the reference device which do not have a sensing layer by normalized to maximum intensity of spectra of sensitizing devices. The red spectrum is determined by detraction the calculated green spectra from the original EL spectra. Figure 2.7 shows the exciplex forming host system and the spectrum of CBP system also determined as same methods. For both of systems, the red emission is considered as probed excitons in the location in EML by Forster energy transferred.

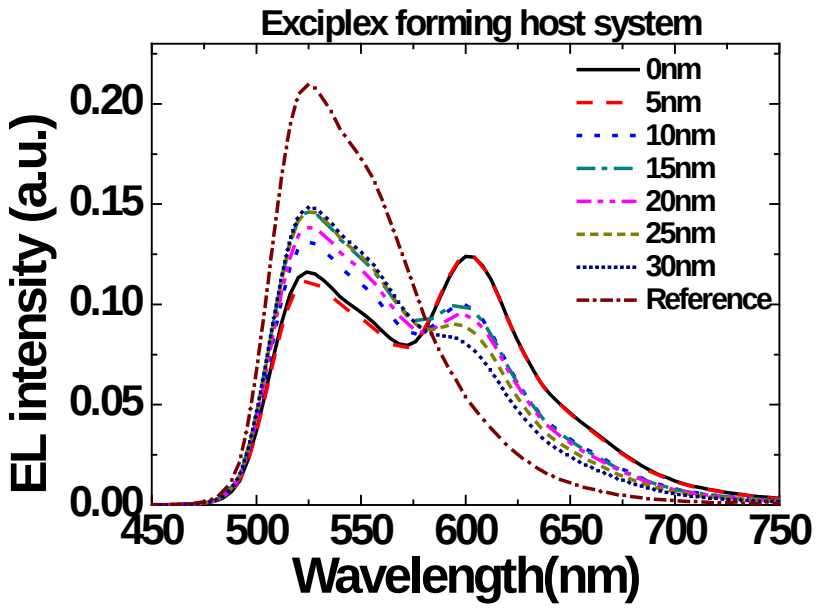

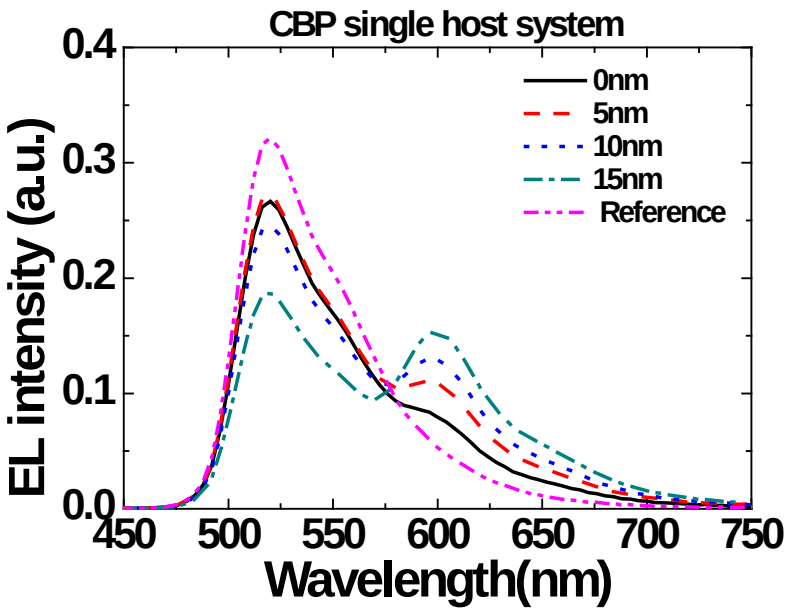

Figure 2.6. The EL spectra of the exciplex forming system and CBP single host system.

(a)

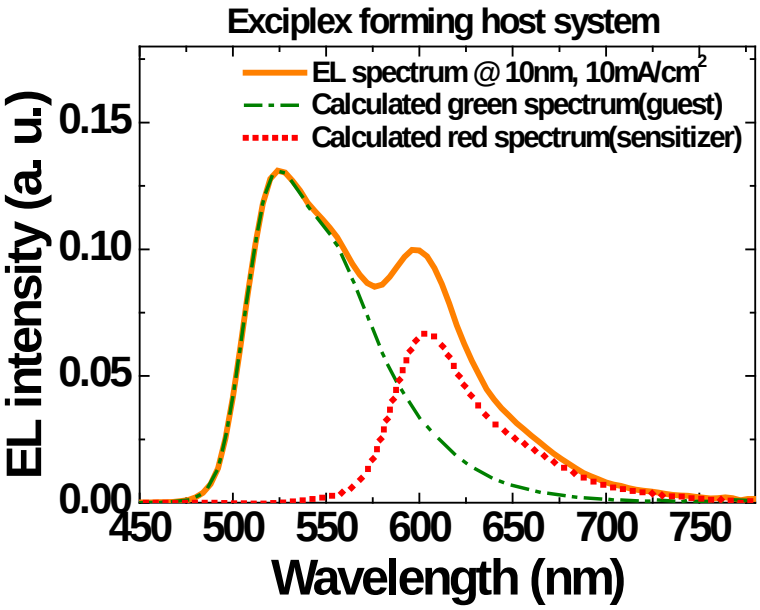
Exciplex forming host system
EL spectrum @ 10nm, 10mA/cm2
Calculated green spectrum(guest)
Calculated red spectrum(sensitizer)
EL intensity (a. u.)
0.00
0.05
0.10
0.15
450
500
550
600
650
700
750
Wavelength (nm)

(b)

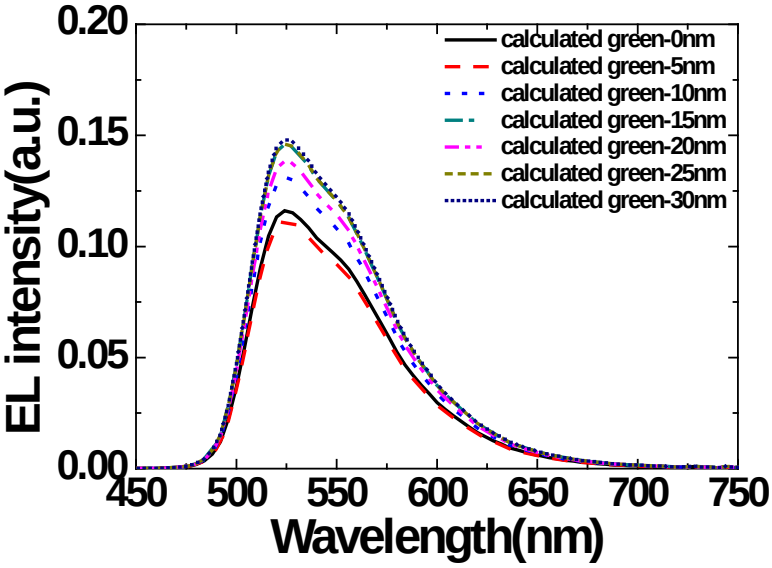
calculated green-0nm
calculated green-5nm
calculated green-10nm
calculated green-15nm
calculated green-20nm
calculated green-25nm
calculated green-30nm
EL intensity(a.u.)
0.00
0.05
0.10
0.15
0.20
450
500
550
600
650
700
750
Wavelength(nm)

(c)

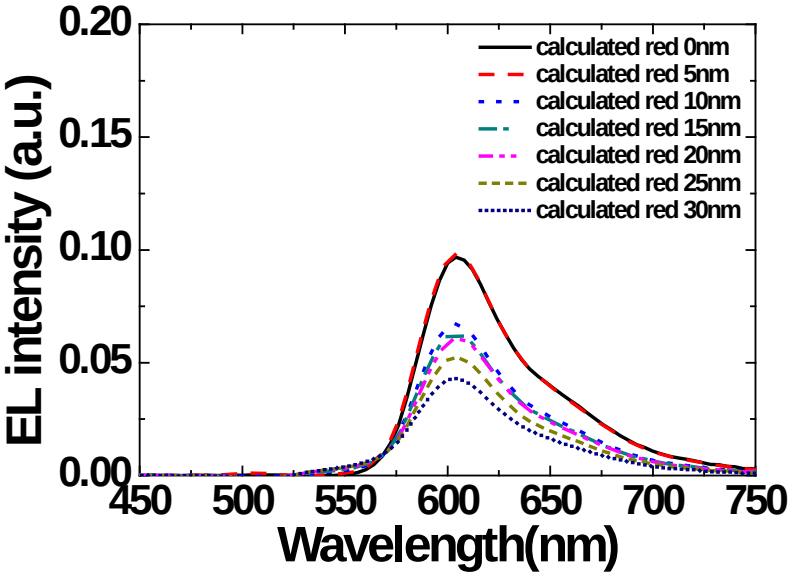

Figure 2.7. The EL spectra is divided into green emitting spectra and red emitting spectra. (a) The orange real line represent EL spectrum of exciplex forming host system at 10mA/cm2 with a sensing layer located at 10nm. (b) Green emitting spectra from EL spectrum. (c) Red emitting spectra from EL spectrum.

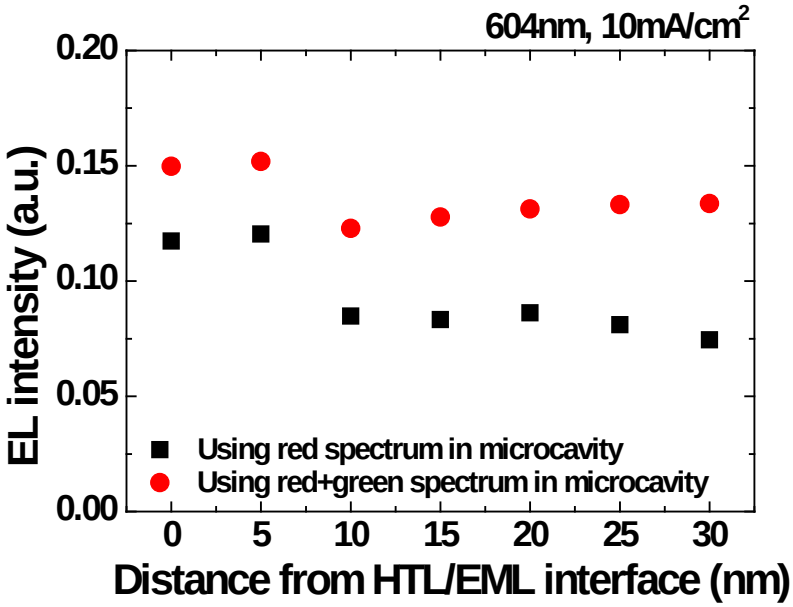

Figure 2.8. The EL intensity of exciplex forming system with distance from HTL/EML interface. To determine the exciton profile precisely, only red spectrum should be used.

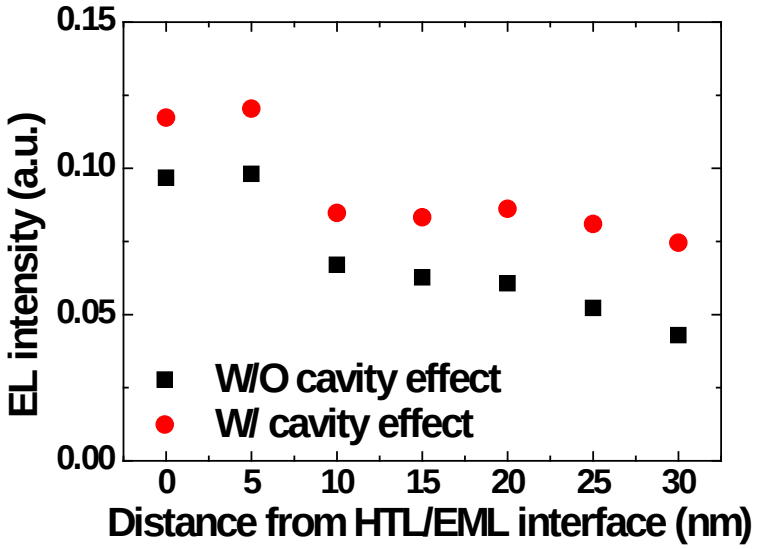

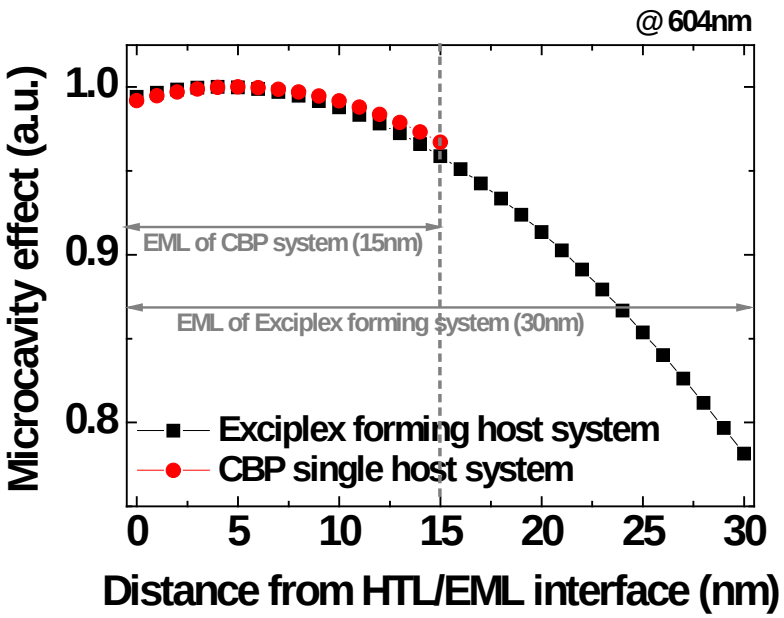

Figure 2.9. (a) The exciton profile with consideration of a microcavity effect and without a microcavity effect. (b) The microcavity effect in a device based on the exciplex forming host

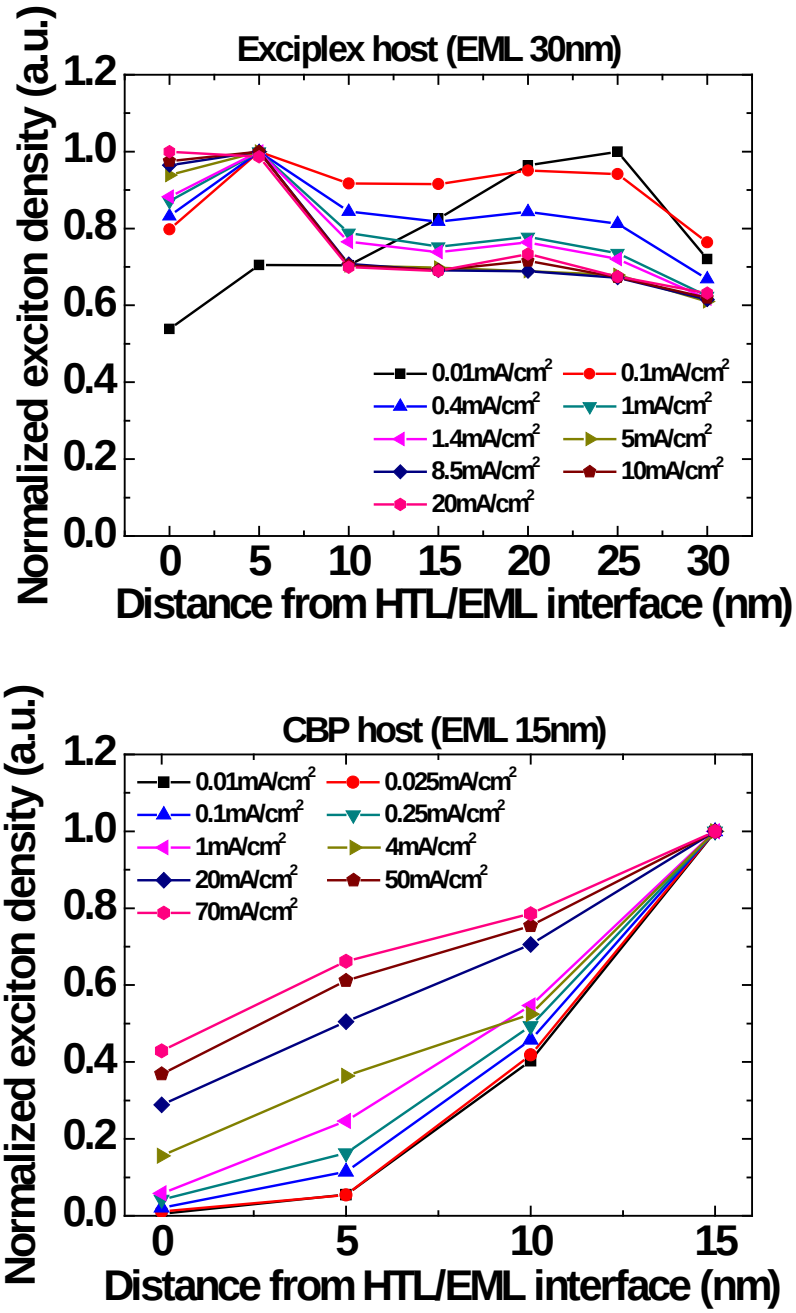

Figure 2.10. (a) The exciton profile in EML using exciplex forming co-host and (b) CBP single host system.

Figure 2.8 shows the exciton profile from above measurements that including the microcavity effect. The emission profile from original spectra in figure3.6 is represent as closed circle symbols and the exciton profile using calculated red spectra is represented as closed rectangular symbols. It is clearly shown that there is significant differences between exciton profile and emission profile from EL spectra of the sensitized devices. Therefore, the spectra of red emission should be used to get accurate exciton profile.

Figure 2.9 shows the exciton profiles in EML of the exciplex forming co-host system. The exciton profile with including the microcavity effect is represented as closed circles and without the microcavity effect as closed rectangular, respectively. The exciton profiles affected by the microcavity effect and it depends on position of excitons. The exciton profile shows more planer than profiles of without consideration of the cavity effects.

Figure 2.10 shows the exciton profile in EML of the exciplex forming co-host system (a) and CBP single host system (b) as function of current density. As expected, the exciton profile of the exciplex forming host system is the most weighted at low current density (0.01mA/cm^2). As current density goes up, the exciton distribution looks even until 0.4mA/cm^2. When the current density is higher than 1mA/cm^2, the excitons are more distributed at HTL side. However, it shows that excitons are more distributed near HTL/EML interface. It is because

that $Ir(ppy)_2acac$ molecules have an effect as hole trap. The hole mobility is lower than electron mobility when dopant existed in TCTA:B3PYMPM host (exciplex forming host). It explains that excitons are distributed more at HTL side than ETL side. These are significantly related to the tendency of EQE roll-off. At low current density, EQE is going up and then it shows maximum EQE when the exciton distribution is well balanced. After the point, the EQE is decreasing with uneven distribution of excitons in EML. To investigate the correlation factor between the exciton profiles and the efficiency roll-off, the theoretical analysis should be conducted.

For the exciton profile of the CBP single host system, the excitons are distributed on ETL side for all current densities. This is because the EML is composed of only a host matrix, CBP which is widely used HTL materials. CBP matrix have a role as a hole transporting rather than electron transporting, the formed excitons are more located at ETL side rather than HTL side. When the current densities are increased, the excitons are more distributed uniformly. That is because the trapped holes are well recombined with injected electrons when the current densities are increased [34].

2.5 Conclusion

In this chapter, the exciton profiles of exciplex forming co-host system and CBP single host system are determined. To investigate precisely, first of all, the emission profile in EML was measured by the sensing layer methods using a red emitting sensitizer. With the spectra from the sensing layer method, the green emission spectra and red emission spectra was divided to ensure sensing of excitons at the locations. With this analysis, the microcavity effect is also considered. To calculate the microcavity effect, a dipole model inside a cavity structure was explained and the correlation between the measured intensity and the located excitons was explained.

Moreover, to fulfill conditions of the sensing layer method, the Forster radius was calculated with equation (2) and J-V properties of the 8 different fabricated samples are shown.

As a result, the exciton profiles of the exciplex forming co-host system and the CBP single host system were investigated. For the exciplex forming system, the excitons are distributed more uniformly compare to that of CBP system. At high current densities levels, the excitons maintain the distribution at the exciplex forming systems, while the excitons distribution was changed at the CBP matrix.

Chapter 3

Combined electrical and optical analysis of the efficiency roll-off in OLEDs

3.1 Introduction

The efficiency roll-off at high current densities are mainly explained by bimolecular nonradiative exciton quenching and charge carrier imbalance between the numbers of electrons and holes in the emission layer (EML). The quenching processes have been studied by many groups because it has been focused on the role of quenching as the main sources of efficiency roll-off, with triplet-triplet annihilation and triplet-polaron quenching as mentioned in chapter 1 [7-8].

Besides quenching of excitons, the exciton generation efficiency also have an effect on efficiency roll-off. Using the electrically driven photoluminescence spectroscopy, the quantitative contributions of exciton quenching and charge carrier imbalance to efficiency roll-off can be measured [9]. Two devices which have same dopants but different device structure are studied as same as chapter 2; exciplex forming co-host system (TCTA:B3PYMPM) and CBP single host system [3,5,11].

In this chapter, the description of measurement concept and theory will be introduced. Also, the detailed experimental set-up and the results will be discussed at end of this chapter.

3.2 Theory

The theoretical models for emission mechanisms in phosphorescent OLED have previously been developed [9]. To describe the exciton physics in OLED device, the model from S. R. Forrest et al. is adapted [9]. It provides a means to quantify the quenching rate and charge balance rate as a function of current density. However, the model did not considered microcavity effect such as effective quantum efficiency and out-coupling efficiency as function of location of excitons. In addition, they assume the exciton profile as a constant with function of location of excitons in EML. Moreover, the calculated charge balance factor is normalized to that of maximum EQE with assumptions that there are no quenching and unit charge balance factor at maximum EQE as function of current density. In this regards, the model is modified including the cavity effect and exciton profiles minimizing the assumptions. From the modified model, the charge balance factor is calculated without normalization.

The total light emitting exciton density, N(x,t,J) in the EML is

represented by

$$N(x,t,J) = N_{EL}(x,t,J) + N_{PL}(x,t,J) \tag{7}$$

Where N_{EL} is electrically generated exciton density in steady-state condition. N_{PL} is optically generated exciton density excited by an optical pulse.

The time dependence of N(x,t,J) is as follows:

$$\frac{d}{dt}\left[N(x,t,J)\right] = G(\mathrm{x,t,J}) - \mathrm{N(x,t,J)}\left[\frac{1}{\tau} + K_Q(x,t,J)\right] \tag{8}$$

Where G(x,t,J) is the electrical generated rate of triplet excitons at current density J and position of EML in x. τ is the lifetime of triplet excitons in device structure. K_Q(x,t,J) is quenching rate followed by all possible monomolecular and bimolecular processes such as triplet-triplet exciton annihilation (TTA) and triplet-polaron quenching (TPQ). It is expressed as

$$K_Q(\mathrm{x,t,J}) = k_{TPQ,\mathrm{n}}[n(x,\mathrm{t,J})] + k_{TPQ,p}[p(x,t,J)] + \frac{1}{2}k_{TTA}[N(x,\mathrm{t,J})]_{\mathrm{EL}} \tag{9}$$

Assume that field induced quenching and joule heating is negligible in this work because that are normally accounts efficiency roll-off in

florescent device [6].

It can be assumed that there is no TTA with PL decay only. The assumption is verified experimentally by showing monoexponential decay with no electric pulsed added.

For steady-state electrical condition, electrically generated exciton density is represented as

$$N_{EL}(x,J)=\frac{G_{EL}(x,J)}{\left[\frac{1}{\tau}+K_Q(x,J)\right]} \tag{10}$$

The total generation rate in the EML is thus

$$\int G_{EL}(x,J)dx=\frac{J_{Cn}-J_{An}}{e}=\frac{J_{Ap}-J_{Cp}}{e}=\frac{Jb(J)}{e}=b(J)\int g_{EL}(x,J)dx \tag{11}$$

$$G(x,J)=b(J)g(x,J) \tag{12}$$

Where g is the normalized exciton generated rate in the emitting layer that explains the exciton profiles in EML.

When charge balance factor=1, $G(x,J)=g(x,J)$ (13)

Charge balance factor, $b=\frac{J_{Cn}-J_{An}}{J}=\frac{J_{Ap}-J_{Cp}}{J}$ (14)

Where J_{An}(J_{Ap}) and J_{Cn}(J_{Cp}) are the electron and hole current densities at the anode and cathode sides of the EML, respectively. Since the exciton density is proportional to EL intensity,

$$I_{EL}(J) = \int N_{EL}(x, J) q_{eff}(x) \eta_{out}(x) dx \tag{15}$$

$$q_{eff}(x) = \frac{qF(x)}{1 - q + qF(x)} \tag{16}$$

$$\eta_{out}(x) = \frac{P_{out}(x)}{P(x)} = \frac{F_{out}(x)}{F(x)} \tag{17}$$

$$\text{Purcell factor, } F(x) = \frac{P(x)}{P_0(x)} \tag{18}$$

$$\text{Purcell factor for out-coupled power, } F_{out}(x) = \frac{P_{out}(x)}{P_0(x)} \tag{19}$$

Where q_{eff}, η_{out} are represented as effective radiative quantum efficiency and out-coupling efficiency, respectively.

Substituting Eq.(10) and Eq.(11) into Eq.(15), we obtain

$$I_{EL}(J) = \int \frac{G_{EL}(x, J)}{\left[\frac{1}{\tau} + K_Q(x, J)\right]} q_{eff}(x) \eta_{out}(x) dx = b(J) \int \frac{g_{EL}(x, J)}{\left[\frac{1}{\tau} + K_Q(x, J)\right]} q_{eff}(x) \eta_{out}(x) dx \tag{20}$$

For simplicity, we assume that K_{tot} include all possible quenching in total EML,

$$K_{tot}(J) = \int_0^{EML} K_Q(x, J)dx \tag{21}$$

Substituting these expressions into Eq.(20) yields

$$I_{EL}(J) = \frac{b(J)}{\frac{1}{\tau} + K_{tot}(x, J)} \int g_{EL}(x, J) q_{eff}(x) \eta_{out}(x) dx \tag{22}$$

The EL intensity of OLED is proportional to EQE, we obtain

$$EQE(J) = \frac{I_{EL}}{J / e} = \frac{\text{\# of out-coupled photons}}{\text{\# of injected electrons}} \tag{23}$$

$$EQE(J) = b(J) \frac{1/\tau}{\left[\frac{1}{\tau} + K_Q(x, J)\right]} \int g_{EL}(x, J) q_{eff}(x) \eta_{out}(x) dx \tag{24}$$

$$EQE_{\max} = \int g_{EL}(x, J) q_{eff}(x) \eta_{out}(x) dx \tag{25}$$

$$\text{Quenching factor(J)} = \frac{\eta_{radiative}}{\eta_{radiative} + \eta_{nonradiative}} = \frac{1/\tau}{\left[\frac{1}{\tau} + K_Q(x, J)\right]} \tag{26}$$

The maximum EQE is calculated using optical simulation to get effective radiative quantum efficiency and out-coupling efficiency as well as measured exciton profile in chapter 3.

Therefore, the experimentally measured EQE(J) is represented by charge balance factor, quenching factor and maximum EQE. Owing to

the unknown variables are charge balance factor and quenching factor, if the quenching factor is achieved, the charge balance factor can be calculated. To get the quenching factor, electrically driven transient PL analysis is conducted with below equations.

$$\frac{dN_{PL}}{dt} = -N_{PL}\left[\frac{1}{\tau} + K_Q(x,J)\right] \tag{27}$$

$$N_{PL}(x,t) = N_{PL}(x,0) \times \exp\left[-t\left(\frac{1}{\tau} + K_Q(x,J)\right)\right] \tag{28}$$

$$\begin{aligned} I_{PL}(t) &= \int N_{PL}(x,t) q_{eff}(x) \eta_{out}(x) dx \\ &= \exp\left(-\frac{t}{\tau}\right) \int N_{PL}(x,0) \exp[-K_Q(x,J)t] q_{eff}(x) \eta_{out}(x) dx \end{aligned} \tag{29}$$

The time resolved changes of optically generated exciton is represented in Eq.(27). As the same way with EL, the intensity of optically generated exciton is represented as in Eq.(29).

With the optical excitation profile, $I_{ex}(x)$, we obtain biexponential decay for the OLED PL transient as the following

$$I_{PL}(t) = \exp\left(-\frac{t}{\tau} - K_Q(x,J)t\right) \int I_{ex}(x) q_{eff}(x) \eta_{out}(x) dx \tag{30}$$

$$I_{PL}(t) = c\left\{\begin{aligned} &\exp\left(-\frac{t}{\tau}\right)\int_0^A I_{ex}(x) q_{eff}(x) \eta_{out}(x) dx + \exp\left[-\left(\frac{t}{\tau}\right)\right]\int_A^B I_{ex}(x) \exp[-K_Q(x,J)t] q_{eff}(x) \eta_{out}(x) dx \\ &+ \exp\left(-\frac{t}{\tau}\right)\int_B^{d_{EML}} I_{ex}(x) q_{eff}(x) \eta_{out}(x) dx \end{aligned}\right\} \tag{31}$$

Where c is normalized factor from proportionality of N(x,0) and $I_{ex}(x)$. For optically excited exciton distribution, it is different with electrically excited exciton distribution. Therefore width of recombination zone cannot be same from width of sensing layer method. Here, $I_{ex}(x)$ is calculated by transfer-matrix method according to the materials properties for the excitation wavelength (337nm). Since all variables are known except quenching factor, K, we can obtain K from fitting to Eq.(31) yield K(J) as a function of drive current.

3.3 Experimental

The two types of OLEDs were fabricated by thermal evaporation onto cleaned glass substrates pre-coated with 70nm thick ITO. Prior to thermal deposition of organic layers, the ITO substrates were exposed to UV-ozone flux for 10 minutes following degreasing in acetone and isopropyl alcohol. All layers were grown by thermal evaporation at a vase pressure of $<10^{-7}$torr without breaking the vacuum. The energy levels of the organic materials were obtained from the reported data.

(a)

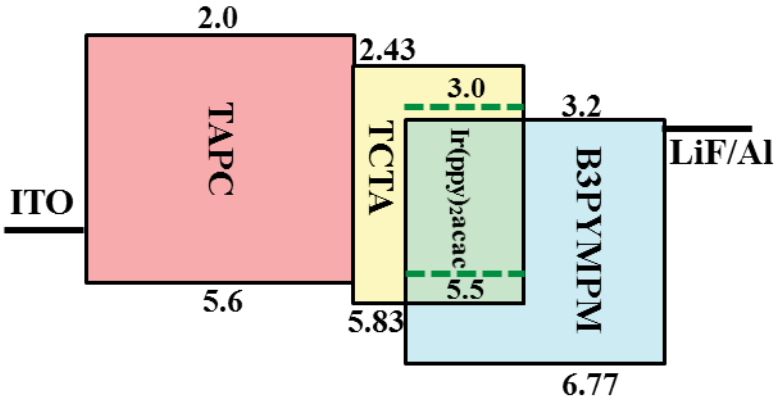

(b)

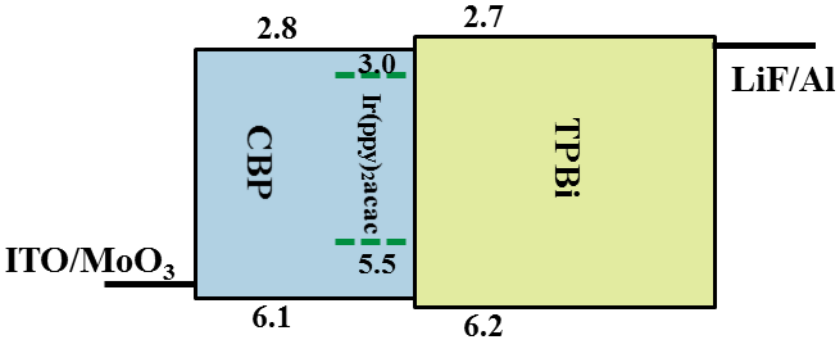

Figure 3.1. (a) The exciton profile in EML using exciplex forming co-host and (b) CBP single host system.

The device structures are shown in Fig 3.1. In the exciplex forming co-host device, a 30nm thick co-deposited TCTA and B3PYMPM layer serves as EML. In CBP single host device, a 15nm thick CBP is served as EML [3,5,11].

The current density, luminance, and EL spectra were measured using a Keithley 2400 programmable source meter and a SpectraScan PR650(Photo Research). The EQE and the power efficiency of the OLEDs were calculated from the current density, luminance, EL spectra, and angular distribution of the EL intensity data.

Electrically pulsed transient PL

To investigate the efficiency roll-off for OLEDs in detail, the electrically pulsed transient photoluminescence spectroscopy was performed in dependence of the current density through the device [9,13]. Conceptually, we follow the ways presented by S. R. Forrest et al.[9]. In addition to a 100μs of longer rectangular electrical pulse applied to the OLED, a stimulation to photoluminescence (PL) in the middle of the electrical pulse. A schematic illustration of the set-up is shown in Fig. 4.2. By analyzing the radiative decay time of the PL signal as a function of the applied current density, the charge balance factors and quenching factors can be identified as explained in chapter 3.2.

The electrical excitation is applied by a pulse generator from DG645. To ensure steady-state conditions, the electrical pulse width of 100μs is chosen at repetition rate of 20 Hz. The optical excitation of the emission layer is applied with a nitrogen laser at normal incidence (wavelength of 337nm). The laser pulse was added to arrive in the middle of each electrical pulses. The emitted light is collected in the direction of the surface normal using a concave lens and a temporal and spectral analysis is performed using a streak-camera system combined with a spectrograph. The pulse of optical and electrical signal and the trigger of streak-camera are combined to pulse delay generator (DG645) to set identical timeline. Integration over the emission spectrum results in the PL decay as a function of time under different applied current densities. Fig. 3.2 (b) illustrates the transient behavior of the PL decay for different current densities. The pulse sequence was performed on the exciplex forming co-host OLEDs. The dashed lines represent the electrical pulse and laser pulse is located at middle of the voltage pulse.

Fig. 3.2 (a) shows schematic of the experimental setup. The pulse delay generator is triggering N_2 laser, electrical pulse and streak camera simultaneously. The output of N_2 laser is placed onto active area of the device. The light is collected from normal direction with concave lens and fiber which connect to streak-camera.

(a)

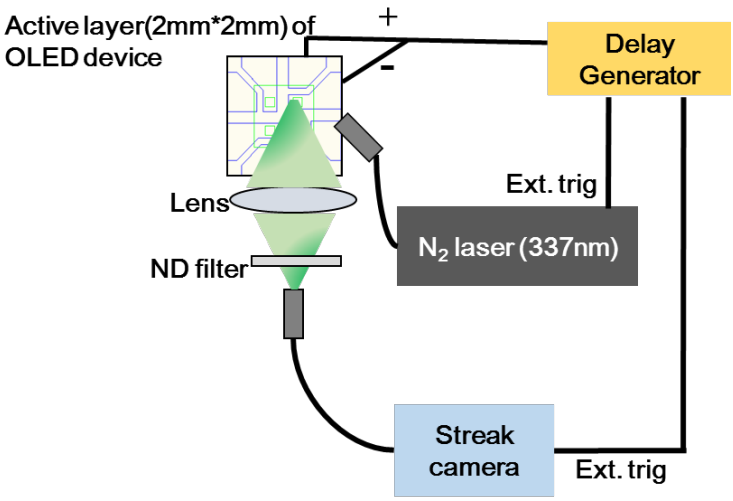

(b)

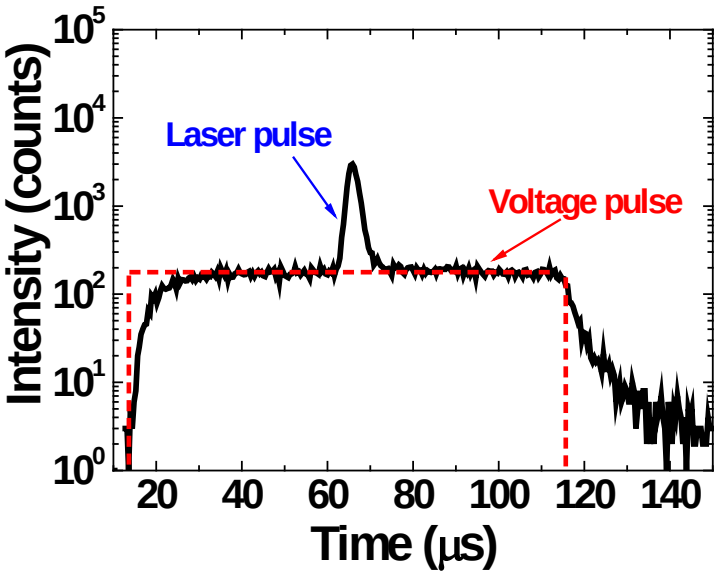

Figure 3.2. (a) The experimental set-up of electrically pulsed transient PL. (b) Illustration of an exemplary pulse sequence. The dashed lines represent the electrical and optical pulse.

3.4 Result and Discussion

Figure 3.3 shows absorbed exciton density distributions by optical pulse at 337nm in the two types of devices. In the exciplex forming co-host system, TCTA which used for HTL absorbed many excitons on the layer than EML by 337nm of optical stimulation as illustrated in Fig.3.3 (a). In CBP single host system, CBP which used for HTL and EML absorbed many excitons which is result for high CBP intensity when optical pulse is applied. The optically generated exciton distribution is calculated by transfer-matrix methods. The calculated results are substituted in $I_{ex}(x)$ in Eq. (31).

Figure 3.4 shows calculated optically generated excitons distributions, effective radiative quantum efficiency and out-coupling efficiency in EML of the exciplex forming host system (squares) and CBP single host system (circles), respectively. With the calculated data, the intensity of optically generated excitons are obtained in Eq.(31).

Figure 3.5 shows the PL transient data as a function of current density for each of the two devices (black and gray lines), as well as the corresponding fits to Eq.(31) (red dashed lines). In figure 3.5 (a), a little amount of quenching is observed in exciplex forming system at increasing current densities as indicated by the reduced effective lifetime. The natural lifetime of $Ir(ppy)_2acac$ is about 1.4μs in the

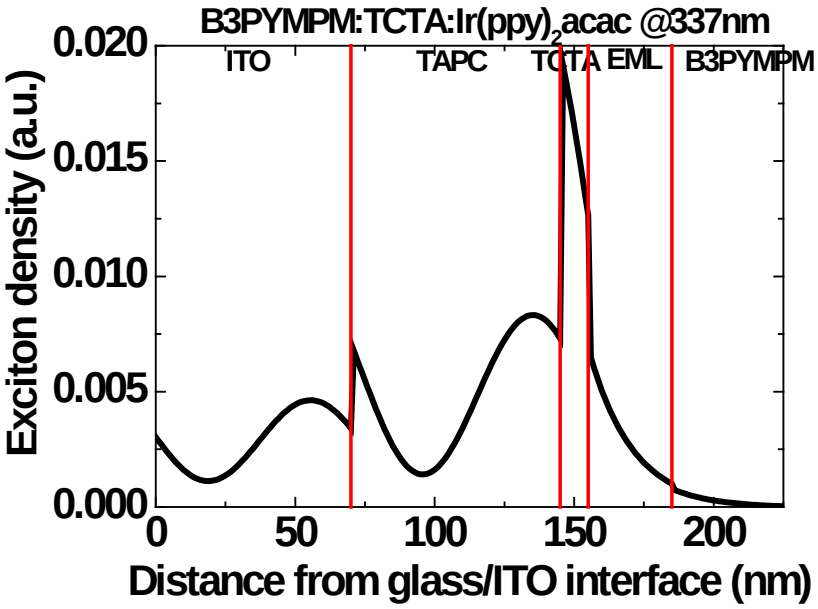

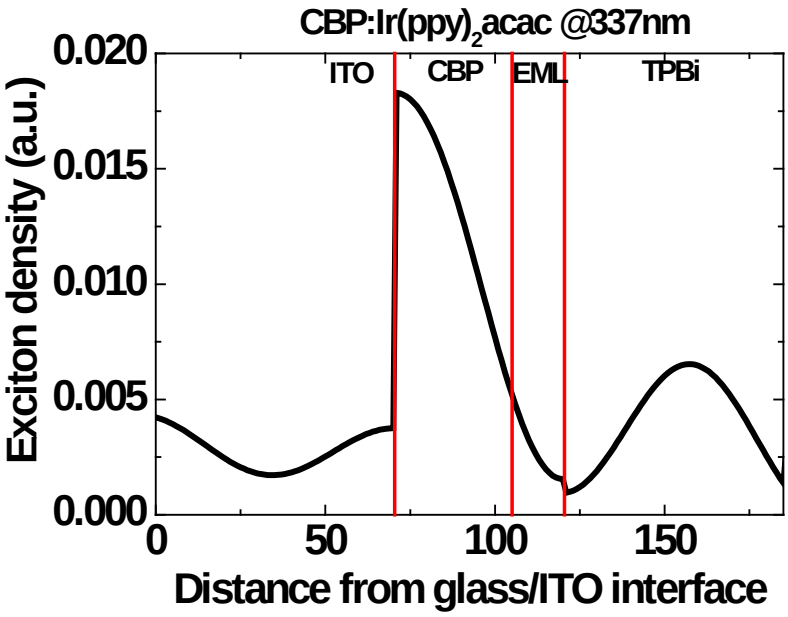

Figure 3.3. The optically generated exciton density distribution in the two systems at 337nm (excited by N_2 laser).

absence of cavity effects (30nm of film condition). When the dopant is located inside a cavity structure, the lifetime is shown as 0.97μs in the device structure based on exciplex forming co-host system and 0.84μs based on CBP single host system. The difference of lifetime in device structures is mainly from a microcavity effect. The total thickness of the systems are 330nm for exciplex host system and 285nm for CBP single host system in this work. Also, the absorption properties and different refractive indexes affect the cavity effect as well.

$$\tau^{*}_{Effective}(J) = \frac{1}{\left[\frac{1}{\tau} + K_Q(J)\right]} \tag{32}$$

In equation (32), the parameter τ*, effective lifetime, represents the exciton lifetime at given driving conditions and is closely correlated to quenching factor as explained in 3.2 [35]. At higher current density level, the increased quenching factor is incorporated into the decreased lifetime. In exciplex forming co-host system, the effective lifetime is decreased to 0.9μs at J=25mA/cm^2 (K_Q=0.925) while in CBP single host system, the effective lifetime is decreased to 0.73μs at J=30mA/cm^2. The transient PL data was fitted with equation (31) for all current density to achieve quenching factor, K_Q, as function of current density. To investigate the quenching factors precisely, the width of recombination zone and the exciton profile are measured from exciton profiles that is studied in chapter 3.

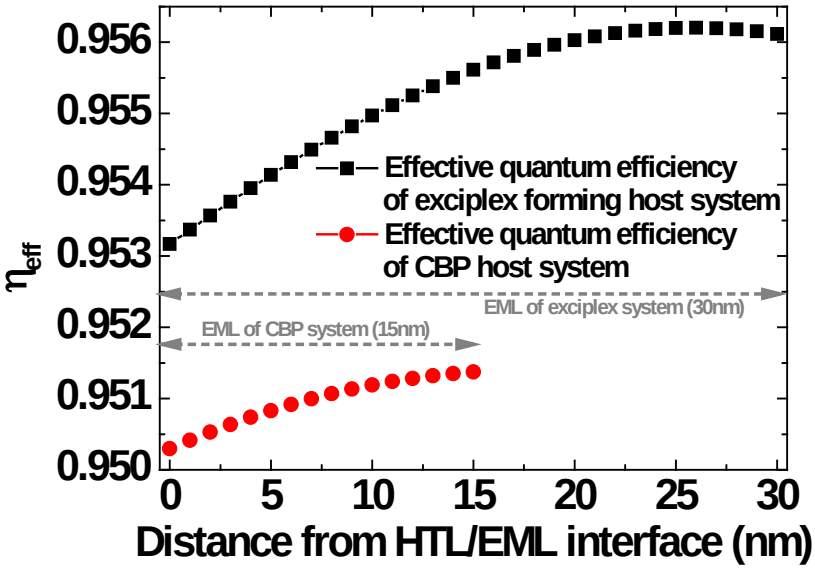
0.956
0.955
0.954
0.953
0.952
0.951
0.950
η_{eff}
Effective quantum efficiency of exciplex forming host system
Effective quantum efficiency of CBP host system
EML of exciplex system (30nm)
EML of CBP system (15nm)
0
5
10
15
20
25
30
Distance from HTL/EML interface (nm)

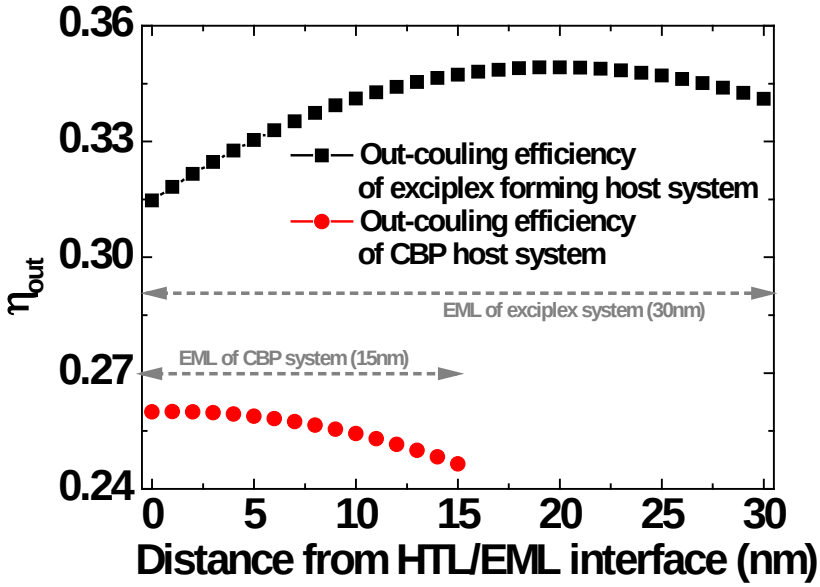
0.36
0.33
0.30
0.27
0.24
η_{out}
Out-couling efficiency of exciplex forming host system
Out-couling efficiency of CBP host system
EML of exciplex system (30nm)
EML of CBP system (15nm)
0
5
10
15
20
25
30
Distance from HTL/EML interface (nm)

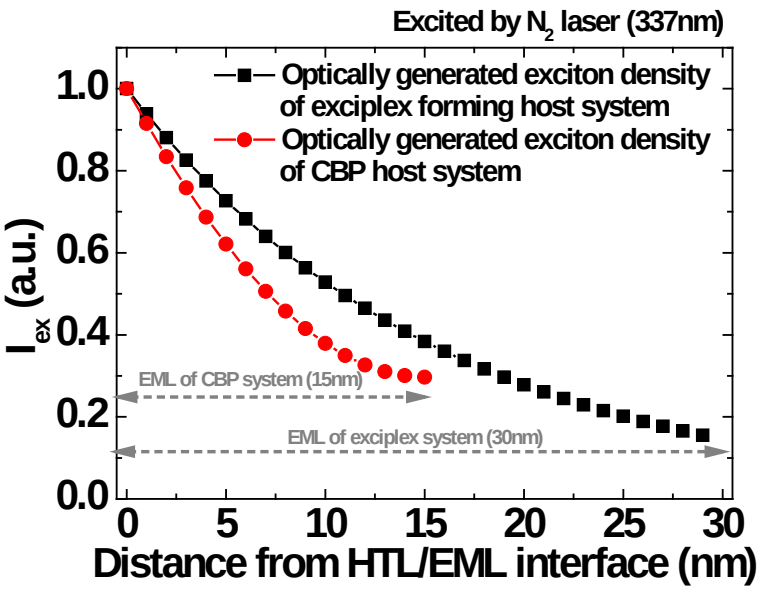

Figure 3.4. The calculated effective radiative quantum efficiency, out-coupling efficiency and optically generated exciton distributions in EML for the two types of devices.

Figure 3.6 shows the EQE roll-off of the two systems in terms of the quenching factor and the charge balance factor of Eq. (24). Measured EQE data are shown as closed rectangular, and open circles depict the theoretically calculated maximum EQE which including the measured exciton profiles, calculated effective quantum efficiency and out-coupling efficiency as function of current density and location of excitons in EML. According to Eq. (24), any difference between measured EQE and maximum EQE must be due to the effect of quenching factor (open upside triangles) and charge balance factor (open downside triangles). Quenching is minor factor to decline EQE at high current density level in exciplex forming host system and it is contribute only higher current density at $J>20mA/cm^2$. However, charge balance factor is increased until the device shows their maximum EQE at $J<1.5mA/cm^2$ from 0.86 to 0.97 and then charge balance is decreased to 0.88 with current density of $25mA/cm^2$. Therefore, the EQE roll-off of exciplex forming co-host system is mainly controlled by charge balance of the device rather than quenching.

In figure 3.6 (b), the EQE roll-off of CBP single host system is shown. The quenching factor is consistently reduced with increasing current density and charge balance factor plays a role only after higher current density $J > 10mA/cm^2$. In CBP single host system, the EQE roll-off is mainly due to both of loss of charge balance and quenching at high

current density. However, at low current density $J<1mA/cm^2$, the reduced EQE with current density is must be due to quenching rather than charge carrier imbalance. Therefore, the EQE roll-off of CBP single host system is mainly controlled by both of charge imbalance and quenching of the device.

This results is able to be well explained with the width of recombination zone and exciton confined system. In exciplex forming co-host system, the high charge balance was maintained at high current density. It is mainly contributed from large gap of energy barriers between HTL and EML. The formed excitons in EML are able to escape from the EML because the gap of energy barrier is higher than 0.6eV which is large enough confine excitons in the EML. In addition, the large width of recombination zone in the EML of exciplex forming co-host system affect to less polaron or exciton density in the EML. The density of molecules in the EML is one of important factors to bimolecular quenching which makes efficiency roll-off. Therefore, the high charge carrier balance and less quenching rate is the origin of low efficiency roll-off of exciplex forming co-host system.

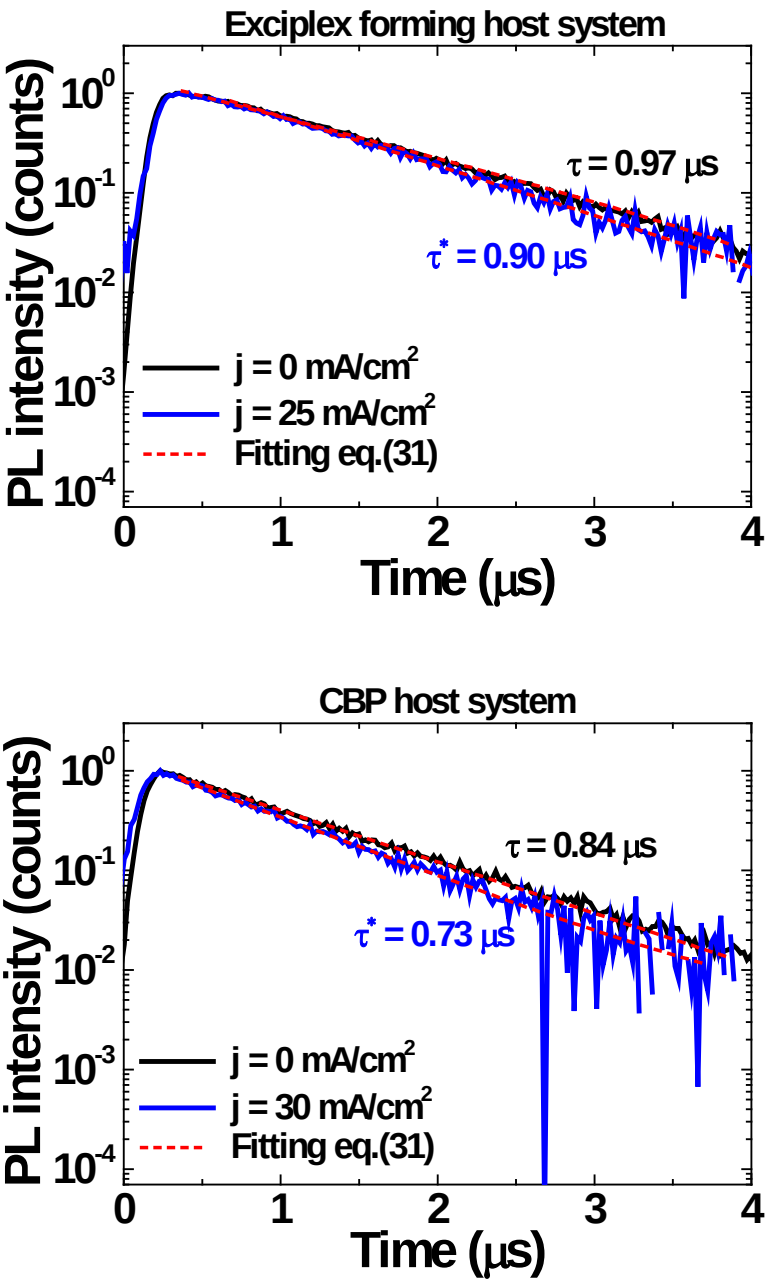

Figure 3.5. The electrically driven photoluminescence transient decay of the two systems of the exciplex forming host system and CBP host system (black and gray line) and the fits according to Eq. (31) of the text (red dashed lines)

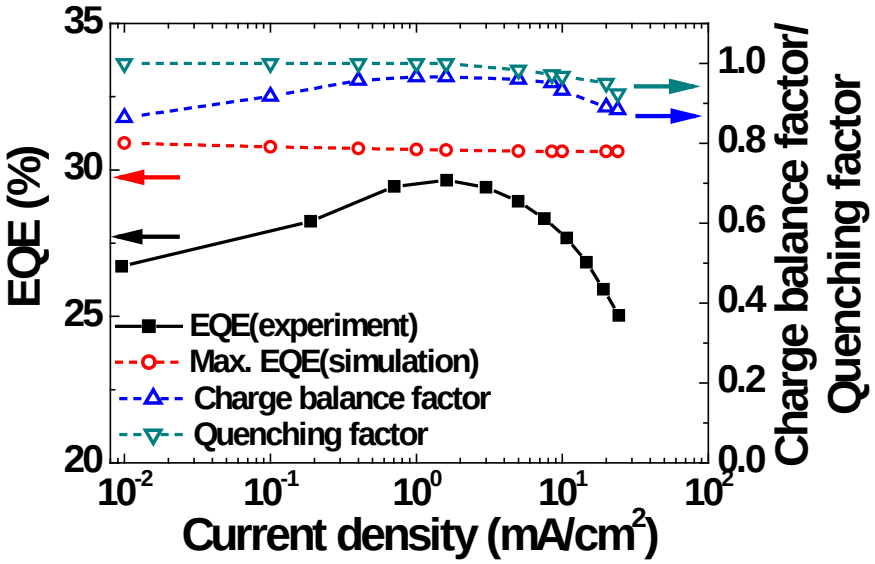

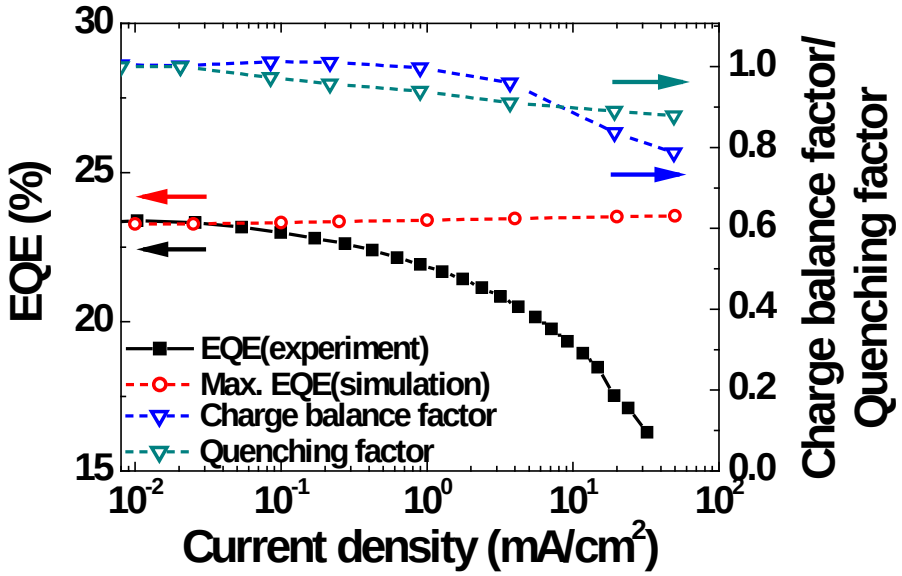

Figure 3.6. External quantum efficiency (EQE) roll-off in the two systems (a) exciplex forming co-host system. (b) CBP single host system. The figure shows the contributions of total quenching (open downside triangles) and loss of charge balance (open upside triangle).

In CBP single host system, there are much trapped charge carriers on the dopant sites in CBP single host system [34]. That is because the recombination mechanism of CBP single host system is mainly due to trap-assisted recombination. Therefore, it is well explained that the quenching factor in decreased at all current densities which means increased quenching from trapped hole on dopant site. In addition, the Pool-Frankel constant (β) of the TPBi layer is more than three times higher than that of the CBP layer, indicating that electrons are well recombine at the CBP side very well at high current density. With no barrier at CBP/EML interface, many electrons distributed at CBP and it result for increasing CBP emission of EL spectra at high current density in figure 3.7 (b). Therefore, the reduced charge balance and increased quenching rate is mainly contribute to efficiency roll-off in CBP single host system.

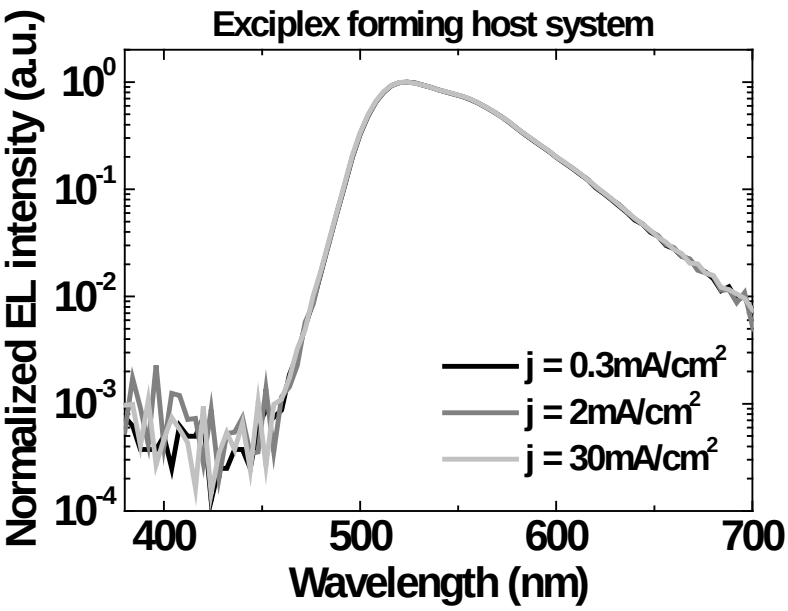

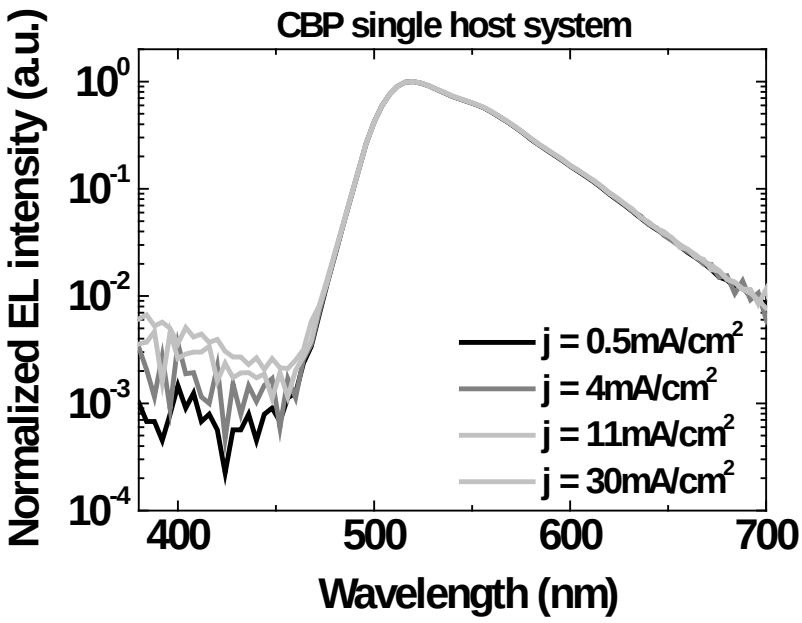

Figure 3.7. Electroluminescence spectra as functions of current density for the (a) exciplex forming co-host system (b) CBP single host system

3.5 Conclusion

In this chapter, the effect of quenching and charge carrier imbalance was measured quantitatively by electrically pulsed transient PL method using modified EQE modeling. First of all, the EQE modeling was discussed theoretically. The measured EQE is represented by quenching factor and charge balance factors with calculated maximum EQE which considered measured exciton profiles and cavity effects. The electrically pulsed transient PL method is processed to calculate the effect of quenching of the exciplex forming co-host system and CBP single host system. The effective lifetime was analyzed to explain the quenching effect because nonradiative decay constant is increased with nonradiative quenching. From the analysis, charge balance factors for the two systems are calculated by Eq. (31). The quenching factors and charge balance factors show different tendencies at the systems as a function of current density that is because of different origin of efficiency roll-off mechanisms. In the exciplex forming co-host system, the high charge carrier balance and less quenching rate with wide recombination zone is the origin of low efficiency roll-off of exciplex forming co-host system. In CBP single host system, the reduced charge balance and increased quenching rate with narrow recombination zone is mainly contribute to efficiency roll-off.

Chapter 4

Summary and outlooks

In this thesis, the origin of efficiency roll-off is analyzed through quantitative measuring the contribution of monomolecular and bimolecular quenching processes and charge carrier imbalance with modeling of EQE including microcavity effects.

In chapter 1, the brief introduction of the organic light emitting diodes and operation principles of OLEDs were described. In addition, the issues in PhOLEDs such as high brightness applications and the downside of phosphorescence emitter were discussed. Also, the processes leading to efficiency roll-off were provided such as bimolecular interaction (TTA, TPQ) and charge carrier imbalance and exciton distribution with current densities.

In chapter 2, the exciton profiles of exciplex forming co-host system and CBP single host system are analyzed. To investigate precisely, first of all, the emission profile was measured by the sensing layer methods using a red emitting sensitizer. Using the spectra from the sensing layer method, the green emission spectra and the red emission spectra was divided to ensure sensing of excitons at the locations. With this analysis, the microcavity effect is also considered. To calculate the microcavity effect, a dipole model inside a cavity structure was explained and the

correlation between the measured intensity and the located excitons was explained. Moreover, to fulfill conditions of the sensing layer method, the Forster radius was calculated with equation (2) and J-V properties of the 8 different fabricated samples are shown. For the exciplex forming system, the excitons are distributed more uniformly compare to that of CBP system. At high current densities levels, the excitons maintain the even distribution in the exciplex forming systems, while the excitons distribution was changed in the CBP matrix.

In chapter 3, the detail theories and experimental methods to quantify quenching and charge balance factor to explain efficiency roll-off was introduced. The combined electrical and optical analysis was used to measure quenching factor. From the quenching factor and exciton profile which is from chapter 3, charge balance factors are calculated with current density. The EQE was represented by quenching factor, charge balance factor and simulated maximum EQE. From the analysis, charge balance factors for the two systems are calculated by Eq. (31). The quenching factors and charge balance factors show different tendencies at the systems that is because of different origin of efficiency roll-off mechanisms. In exciplex forming co-host system, the high charge carrier balance and less quenching rate is the origin of low efficiency roll-off of exciplex forming co-host system. In CBP single host system, the reduced charge balance and increased quenching rate is mainly contribute to efficiency roll-off.

Bibliography

1. C. Tang and S. VanSlyke, Appl. Phys. Lett. 51, 913 (1987).
2. M. Baldo, D. O'brien, Y. You, A. Shoustikov, S. Sibley, M. Thomson and S. Forrest, Nature 395, 151 (1998).
3. Y.-S. Park, S. Lee, K.-H. Kim, S.-Y. Kim, J.-H. Lee and J.-J. Kim, Adv. Funct. Mater. 23, 4914 (2013).
4. S.-Y. Kim, W.I. Jeong, C. Mayr, Y.-S. Park, K.-H. Kim, J.-H. Lee, C.-K. Moon, W. Brutting and J.-J. Kim, Adv.Funct.Mater.23, 3896 (2013).
5. K.-H. Kim, C.-K. Moon, J.-H. Lee, S.-Y. Kim, and J.-J. Kim, Adv. Mater. 26, 3844 (2014).
6. C. Murawski, K. Leo, and M.C. Gather, Adv. Mater. 25, 6801 (2013).
7. M.A. Baldo, C. Adachi, S. R. Forrest, Phys. Rev. B 62, 10967 (2000).
8. S. Reineke, K. Walzer, K. Leo, Phys. Rev. B 75, 125328 (2007).
9. N. C. Giebink and S. R. Forrest, Phys. Rev. B 77, 235215 (2008).
10. N. C. Erickson and R. J. Holmes, Adv.Funct.Mater. 23, 5190 (2013).
11. Z. B. Wang, M. G. Helander, J. Qiu, D.P. Puzzo, M.T. Greiner, Z.W. Lu, Appl. Phys. Lett. 98, 073310 (2011).
12. Y. Zhang, J. Lee and S.R. Forrrest, Nature com. 5 (2014)

13. M. Ichikawa, R. Naitou, T. Koyama and Y. Taniguchi, Jpn. J. Appl. Phys. 40 (2001).

14. C. Adachi, M.A. Baldo, M.E. Thomson, S.R. Forrest, J. Appl. Phys. 90, 5048, (2001).

15. M. Furno, R. Meerheim, M. Thompson, S. Hofmann,, B. Lussem, K. Leo, Proc. SPIE 7617, 76176 (2010)

16. M. Baldo, D. Obrien, Y. You, A. Schoustikov, S. Sibley M. Thompson and S. R. Forrest, Nature 395, 151 (1998). C 118 (2014) 9412–9418.

17. D. Tanaka, H. Sasabe, Y.-J. Li, S.-J. Su, T. Takeda and J. Kido, Jpn. J. Appl. Phys. 46, L10 (2007).

18. M. Helander, Z. Wang, J. Qiu, M. Greiner, D. Puzzo, Z. Liu and Z. Lu, Science 332, 944 (2011).

19. T. Tsutsui, E. Aminaka, C. Lin and D.-U. Kim, Phil. Trans. R. Soc. A 355, 801 (1997).

20. M. Schwoerer, H.C. Wolf, Organic Molecular Sollids, WILEY-VCH Berlag GnbH & Co. KGaA, Weinheim, 2007.

21. S. Reineke, T. C. Rosenow, B. Lussem, K. Leo, Adv. Mat. 22, 3189 (2010).

22. N. Chopra, J. Lee, J. G. Xue, F. So, IEEE Trans. Electron Devices 57, 101 (2010).

23. A. B. Chwang, R. C. Kwong, J.J. Brown, Appl. Phys. Lett. 80, 725 (2002).

24. J.C. Scott, S. Karg, S. A. Carter, J. Appl. Phys. 82, 1454 (1997).

25. B. Ruhstaller, S. A. Carter, S. Barth, H. Riel, W. Riess, J. C. Scott, J. Appl. Phys. 89, 4575 (2001).

26. D. V. Khramtchenkov, H. Bassler, V.I. Arkhipov, J. Appl. Phys. 29, 9283 (1996).

27. N.C. Erickson and R.J. Holmes, Adv. Funct. Mater. 23, 5190 (2013).

28. M. PoPe, C.E. Swenberg, Electronic Processes in Organic Crystals, Oxford University Press, New York

29. N. J. Turro, Modern Molecular Photochemistry, University Science Books, CA 1991.

30. T. Forster, Discuss. Faraday Soc. 1959.

31. C.-K Moon, S.-Y Kim, J.-H Lee, and J.-J Kim, Optics Express 23 7 (2015).

32. B. Perucco, N.A. Reineke, D. Rezzonico, M. Moos, and B. Ruhstaller, Optics Express 18, S2 (2010).

33. S. L. M. van Mensfoort, M. Carvelli, M. Megens, D. Wehenkel, M. Bartyzel, H. Greiner, R.A.J. Janssen and R. Coehoorn, Nature Photonics, 4, 329, (2010).

34. J.-H Lee, S. Lee, S.-J. Yoo, K.-H. Kim, and J.-J Kim, Adv. Funct. Mater, 24, 4681 (2014)

35. S. Mladenovski, S. Reineke, and K. Neyts, Opt. Lett. 34, 1375 (2009)

초 록

인광 염료를 사용 한 유기발광소자는 최근 디스플레이, 조명 관련 응용으로 큰 잠재력을 가지고 있기 때문에 많은 주목을 받고 있다. 인광 염료를 사용 한 유기발광소자의 사용은 100%의 내부 광자 전환 효율을 가질 수 있으며 최대의 외부양자효율 달성이 가능 하므로 중요하다. 하지만 높은 전류밀도에서 외부양자효율이 감소하는 현상이 발생 하는 단점이 있다. 휘도 증가에 따른 외부양자효율의 감소는 이분자 간 상호작용과 전하의 불균형이 원인이 될 수 있다.

이 학위논문에서는 높은 전류밀도에서의 인광염료를 사용한 유기발광 소자의 외부양자효율 저하의 원인을 이분자 간 결합과 전하 불균형의 정량적인 분석을 통하여 규명하고자 하였다. 이 분석에는 미세 동공효과와 발광 층 에서의 엑시톤의 분포를 포함하는 유도된 수식이 사용 되였다. 이 수식을 통하여 외부양자효율의 감소는 이종 분자간 결합에 의한 삼중항 밀도 감소를 의미하는 퀜칭 인자와 전하 균형 인자로 표현 되었다.

전기적, 광학적으로 동시에 여기 된 소자의 시간에 따른 빛

의 강도 감소를 근사하여 퀜칭 인자와 전하 균형 인자를 수식을 통하여 정량적인 양을 계산 하였다. 정밀한 계산을 위하여 발광 층 내부의 엑시톤의 분포를 적색의 감지 층 삽입 방법을 통하여 실험으로 규명하였다.

본 학위 논문에서는 녹색 인광 유기발광소자에서 최고 효율을 달성 한 엑시플렉스 구조와 널리 사용되는 구조인 4,4'-Bis(carbazol-9-yl)biphenyl(CBP)를 단일 호스트를 사용한 구조의 효율저하 현상이 분석되었다. 엑시플렉스 구조를 사용한 인광 유기발광소자의 효율 감소가 적은 원인은 넓은 엑시톤 형성 영역에 의한 높은 전하 균형과 낮은 퀜칭 인자 때문인 것으로 분석 되었다. CBP 단일 호스트를 사용한 인광 유기발광소자의 효율 감소는 좁은 엑시톤 형성 영역에서의 낮은 전하 균형과 높은 퀜칭 인자에 의해 효율이 저하되는 것으로 분석되었다. 동일 염료를 사용한 구조에서 외부양자효율 저하의 원인이 다른 이유는 더 심도 있는 연구를 통하여 밝혀야 할 것이다.

주요어: 엑시플렉스를 형성하는 공동호스트, 유기발광소자, 외부양자효율감소, 엑시톤 분포, 퀜칭 인자, 전하 균형 인자

학 번: 2013 - 23819

List of Publications

- Hyun-Sub Shim , Francis Lin, Jihun Kim, **Bomi Sim**, Tae-Min Kim, Chang-Ki Moon, Chun-Kai Wang, Yongsok Seo, Ken-Tsung Wong, and Jang-Joo Kim, "**Efficient Vaccum-Deposited Tandem Organic Solar cells with Fill Factors Higher Than Singe-Junction Subcells"** *Advanced Energy Materials*, 2015, 1500228.
- Kwon-Hyeon Kim, Chang-Ki Moon, Jin Won Sun, **Bomi Sim** and Jang-Joo Kim, "**Triplet Harvesting by a Conventional Fluorescent Emitter Using Reverse Intersystem Crossing of Host Triplet Exciplex"** *Advanced Energy Materials*, 2015, 1500228.